UCRL-ID-121725

PCMDI
Program for Climate Model Diagnosis and Intercomparison

PCMDI Report No. 28

INTERANNUAL TROPICAL RAINFALL VARIABILITY IN GENERAL CIRCULATION MODEL SIMULATIONS ASSOCIATED WITH THE ATMOSPHERIC MODEL INTERCOMPARISON PROJECT

by

K.R. Sperber[1] and T.N. Palmer[2]

[1]Program for Climate Model Diagnosis and Intercomparison
Lawrence Livermore National Laboratory, Livermore, CA, USA

[2]European Centre for Medium-Range Weather Forecasts
Reading, Berkshire RG2 9AX, United Kingdom

November 1995

PROGRAM FOR CLIMATE MODEL DIAGNOSIS AND INTERCOMPARISON
UNIVERSITY OF CALIFORNIA, LAWRENCE LIVERMORE NATIONAL LABORATORY
LIVERMORE, CA 94550

UCRL-ID-121725

PCMDI
Program for Climate Model Diagnosis and Intercomparison

PCMDI Report No. 28

INTERANNUAL TROPICAL RAINFALL VARIABILITY IN GENERAL CIRCULATION MODEL SIMULATIONS ASSOCIATED WITH THE ATMOSPHERIC MODEL INTERCOMPARISON PROJECT

by

K.R. Sperber[1] and T.N. Palmer[2]

[1]Program for Climate Model Diagnosis and Intercomparison
Lawrence Livermore National Laboratory, Livermore, CA, USA

[2]European Centre for Medium-Range Weather Forecasts
Reading, Berkshire RG2 9AX, United Kingdom

November 1995

PROGRAM FOR CLIMATE MODEL DIAGNOSIS AND INTERCOMPARISON
UNIVERSITY OF CALIFORNIA, LAWRENCE LIVERMORE NATIONAL LABORATORY
LIVERMORE, CA 94550

ABSTRACT

The interannual variability and Reproducibility of rainfall over the Indian subcontinent, the Sahel and the Nordeste region of Brazil have been evaluated from the suite of AMIP simulations. Rainfall variations over the Nordeste region are the most readily captured owing to the intimate link with Pacific and Atlantic SSTs. The precipitation variations over the Indian subcontinent and the Sahel are relatively less well captured by the models respectively. Additionally, an Indian monsoon wind shear index was calculated for each model. The models are generally more adept at simulating the variability of the wind shear index than that associated with the rainfall over this region, indicating that the models exhibit greater fidelity at capturing the large-scale dynamical fluctuations. For each region improved skill scores and enhanced Reproducibility result for those models that qualitatively simulate the observed rainfall/SST correlation pattern which is dominated by an ENSO teleconnection in the Pacific Ocean. Accordingly for this subset of the models, the enhancement in skill and Reproducibility occurred mainly during years of strong El Niño and La Niña conditions. A suite of six ECMWF AMIP runs (differing only in their initial conditions) have also been examined. The Indian monsoon rainfall exhibits a consistent response during 1987 and 1988, while during other years differences are simply not very predictable, possibly because of internal chaotic dynamics that are associated with intraseasonal monsoon fluctuations and/or land surface process interactions. In this case the Reproducibility is poor indicating that the average intra-model spread is greater than the temporal variability of the ensemble mean. For the Sahel and the Nordeste the Reproducibility increases to 2.4 and 9.0 respectively indicating a robust response to the boundary conditions for this model. Five SUNY/NCAR Genesis low resolution initial condition realizations were also examined. In this model the Nordeste rainfall also exhibited the largest Reproducibility, however for all regions the Reproducibility was smaller than that for the ECMWF model.

The relationship of the all-India and Sahel rainfall/SST teleconnections with horizontal resolution, convective closure and numerics has been evaluated. Models with resolution ≥T42 performed more poorly than lower resolution models. The higher resolution models were predominantly spectral. At low resolution, spectral vs. gridpoint numerics performed with nearly equal verisimilitude. At low resolution, moisture convergence closure was slightly preferable other closure techniques. At high resolution, the models that utilized a moisture convergence criteria performed very poorly suggesting that moisture convergence may be inappropriate for models with horizontal resolution ≥T42.

1. INTRODUCTION

It is likely that ensemble techniques will play an essential role in the production of seasonal forecasts from coupled ocean-atmosphere models. As in medium-range prediction (e.g., Molteni et al. 1995), the dispersion of the ensemble is an estimate of the predictability of the atmospheric circulation and associated weather elements. The Atmospheric Model Intercomparison Project (AMIP, Gates 1992) provides a unique opportunity to study the potential predictability of interannual fluctuations of the atmosphere based on ensembles of multi-annual integrations of atmospheric general circulation models (AGCMs). In this project, many of the world's AGCMs have been integrated over the ten year period 1979-1988 with identical specified sea surface temperatures (SSTs). In addition, multiple realizations of the ten-year period have been obtained by running some of the AGCMs from different initial conditions (but with the same SSTs). Each model has a unique set of physical parameterizations; together this ensemble is comprised of integrations made from perturbations to both model formulation and initial conditions.

Estimates of potential predictability (henceforth referred to as Reproducibility) of atmospheric interannual fluctuations can be deduced from the resulting ensemble dispersion. The qualifier "potential" is used since the AMIP experimental procedure implicitly assumes that SST is perfectly predictable. The extent to which this is true can only be demonstrated using coupled ocean-atmosphere models, though for some of the major El Niño events occurring during the AMIP decade, the assumption that tropical SSTs are predictable on seasonal time scales is justifiable (Palmer and Anderson 1994).

If the AMIP ensemble dispersion is small compared to the interannual fluctuations in the ensemble-mean fields, then the SST field can be said to have a reproducible effect on the overlying atmospheric circulations (independent of model formulation or atmospheric initial conditions). Conversely, if ensemble dispersion is large compared with interannual fluctuations in the underlying SST field, then it is possible that the inherent chaotic variability associated with the nonlinear atmospheric dynamics has overwhelmed the impact of variations in the atmosphere's underlying boundary conditions.

It is possible to use the AMIP ensemble to study any component of atmospheric potential predictability in this way. However, in this paper we will focus on the seasonal predictability of rainfall and circulation in three regions (of practical interest) in the tropics: the Indian subcontinent, the African Sahel and the Brazilian Nordeste. The monsoons have proven to be a critical phenomenon in assessing a GCM's ability to simulate tropical climate and variability as demonstrated in the studies organized under the aus-

pices of the Tropical Ocean Global Atmosphere Monsoon Numerical Experimentation Group (TOGA MONEG, WMO 1992, 1993), in particular conditions associated with El Niño and La Niña conditions that tend to be associated with drought and flood conditions over the Indian subcontinent (Ropelewski and Halpert 1987, 1989).

In studying simulated data, it is necessary to be aware of the impact that model error can have on the conclusions obtained from the analysis of this data. In the case of the GCMs studied here, the resulting estimates of climate bias obtained from the ten-year integrations are certainly model dependent. As a result there is a component of ensemble dispersion that is not directly related to intrinsic atmospheric chaotic variability, but rather is associated with model dependent systematic error. In order to isolate model related dispersion from intrinsic atmospheric chaotic variability, a basic "quality control" has been performed on the full ensemble, retaining on those models for which the climate bias is suitably small (based on an objective criteria described in Section 4c). The estimate of ensemble dispersion from this quality controlled sub-ensemble gives a more reliable estimate of internal atmospheric variability. However, even within the sub-ensemble of quality controlled integrations, the model systematic errors are not negligible. To assess the potential problems that may arise, the estimates of potential Reproducibility are compared with skill measures obtained by correlating observed and simulated values of seasonal rainfall and circulation indices.

2. THE MODELS

In this paper we present an analysis of simulations associated with the Atmospheric Model Intercomparison Project (AMIP), a coordinated effort to simulate the 1979-88 decade using standardized boundary conditions with approximately 30 atmospheric general circulation models (Gates 1992). This analysis is based on a monsoon diagnostic proposal to AMIP originating from MONEG. Using monthly mean data from these simulations indices of tropical precipitation have been calculated in an effort to access the performance of the models over the course of the AMIP decade. Phillips (1994) presents a summary documentation of the AMIP models.

Two additional models were incorporated in this study. LMD and SUNY/NCAR submitted additional AMIP integrations with revised models. Relative to their initial AMIP contributions, LMD6 employs a new land surface parameterization called SECHIBA (Ducoudré et al. 1993), and the SUNY/NCAR Genesis 2 (SNG2) model uses a new cloud scheme, and it was run at a lower horizontal resolution to perform five initial condition realizations that will be compared with the multiple ECMWF realizations. Unless other-

wise noted, a single realization from the ECWMF realizations and the SNG2 realizations was chosen randomly for the discussions related to the climatologies, case studies, and interannual indices discussed below.

3. STANDARDIZATION, SKILL SCORES AND REPRODUCIBILITY

a. *Standardization*

In order to account for the different amplitudes of interannual variability among the models, as well as their individual biases in simulating the time-mean field, we have standardized the area-weighted regional indices presented in this paper. For each index, α, simulated and observed, we calculate the time mean of the area-weighted index for years i=1,2,...10 of the AMIP decade:

$$\overline{x_\alpha} = \frac{1}{10}\sum_{i=1}^{10} x_{i\alpha} \qquad (1)$$

and its standard deviation with respect to the time mean:

$$\sigma_{t\alpha} = \left[\frac{1}{9}\sum_{i=1}^{10}(x_{i\alpha} - \overline{x_\alpha})^2\right]^{1/2} \qquad (2)$$

Then the standardized indices are calculated as follows:

$$y_{i\alpha} = \frac{(x_{i\alpha} - \overline{x_\alpha})}{\sigma_{t\alpha}} \qquad (3)$$

The observed and simulated standardized indices are also used for estimation of the Brier skill score and Reproducibility.

b. *The Brier Score*

The Brier score has been used as a measure for assessing NWP performance (Murphy and Katz 1985, Perrone and MIller 1985). In this application it measures the skill of the ensemble of models to simulate the correct sign of an anomaly with respect to observations, irrespective of the magnitude of the simulated departure. (Note: we do however require that the observed standardized departure for a given year i exceed +/- 0.25 to be included in the calculation of the Brier score, in which case the number of years n_y from

which the average Brier score is calculated may be less than 10). The average Brier score is calculated as follows:

$$\overline{Bs} = \frac{1}{n_y} \sum_{i=1}^{n_y} [\,(1.0 - Y_i)^2 + (0.0 - N_i)^2\,] \qquad (4a)$$

which reduces to

$$\overline{Bs} = \frac{1}{n_y} \sum_{i=1}^{n_y} 2N_i^2 \qquad (4b)$$

where:

Y_i = fraction of models simulating an anomaly of the correct sign during year i

N_i = fraction of models simulating an anomaly of the incorrect sign during year i, and $N_i = (1 - Y_i)$

Brier scores may range from 0.0 (a perfect score) to 2.0 (total disagreement with observations). For climatology (Y_i = 0.5, N_i =0.5) the Brier score equals 0.5.

c. *Reproducibility*

While the Brier score is a model-data verification tool, the Reproducibility, which is essentially a signal to noise ratio, is a model-model intercomparison.The realizations intercompared may consist of different models, or multiple realizations of the same model that differ only in the specification of initial conditions. The Reproducibility is a measure of the models' ability to consistently respond to the imposed boundary forcing. Using the standardized indices of each model as calculated from Eq. 3, we calculate the ensemble mean time series over years i = 1, 2,...10 as follows:

$$\langle y_i \rangle = \frac{1}{m} \sum_{\alpha=1}^{m} y_{i\alpha} \qquad (5)$$

where m = the number of models considered. Next, we calculate the variance of the ensemble mean time series:

$$\sigma^2_{tsig} = \frac{1}{9}\sum_{i=1}^{10} \langle y_i \rangle^2 \qquad (6)$$

which is a measure of the interannual variability of the signal extracted from the suite of simulations under consideration. Note: by definition the time mean of $\langle y_i \rangle$ is zero since the standardized indices from Eq. 3 were employed in Eq. 5. σ^2_{tsig} is the numerator of the Reproducibility.

The denominator of the Reproducibility is the average of the variance estimates from each year i for the m prognostications, and it is a measure of the unpredictability of the signal $\langle y_i \rangle$. It is calculated as follows:

$$\overline{\sigma^2_{noise}} = \frac{1}{10}\sum_{i=1}^{10}\left[\frac{1}{(m-1)}\sum_{\alpha=1}^{m}(y_{i\alpha} - \langle y_i \rangle)^2\right] \qquad (7)$$

The Reproducibility R is:

$$R = \frac{\sigma^2_{tsig}}{\overline{\sigma^2_{noise}}} \qquad (8)$$

In the case when denominator equals zero, each realization is an exact replica of the other and the Reproducibility is ∞. Thus, when

$R > 1$, the signal is distinguishable from the noise

$R < 1$, the unpredictable internal variability dominates

4. INDIAN SUMMER MONSOON

a. *1979-88 Climatologies*

The 10-year June-July-August-September (JJAS) averaged climatologies of precipitation and 850hPa flow provide a reference against which the interannual variations of monsoon behavior can be evaluated. From this perspective we may relate biases in the climatologies to errors in the simulation of extreme events such as those associated with

the 1987 and 1988 El Niño and La Niña drought and flood regimes. For the purpose of validation, the precipitation climatology was obtained from a 4^{o} latitude x 5^{o} longitude merged data set that utilized MSU precipitation estimates over the ocean (Spencer 1993) and station raingauge data over land (Schemm et al. 1992; over Antarctica the Legates and Wilmott [1990] data were used) which spanned the AMIP decade. The JJAS station rainfall data was not available for the full 10 years at some land points, primarily in the vicinity of China, and several grid points north and east of the Bay of Bengal, and data was considered to be missing if less than 6 years were available from which to construct the time mean field. ECMWF analyses (1980-89) are used to validate the 850hPa flow. These climatologies are shown in Figs. 1a and 1f respectively. The maxima in precipitation along the west coast of India and that over southwest Asia are associated with the Somali jet and the trough in the Bay of Bengal respectively. A precipitation minimum occurs over the southeastern portion of the subcontinent associated with the rainshadow effect of the western Ghats. Other regional-scale relationships, that are generally ignored when evaluating monsoons simulation, are evident in the precipitation and low-level flow. Principally, northerlies and northwesterlies dominate the low-level flow along the western and southern edge of the Tibetan Plateau (Fig. 1f). Over northwestern India this flow is particularly important since it is associated with advection of dry air from the desert which serves to moderate the availability of precipitable water (Fig. 1a). Similarly, westerlies from the eastern Saudi peninsula influence the precipitation distribution as can be seen by the southwest to northeast orientation of 2mm day^{-1} contour over the Arabian Sea (Fig. 1a).

The precipitation and low-level flow climatologies for several of the model simulations are also presented in Fig. 1. The CCC model Somali jet, Fig. 1g, is well simulated, although it tends to be somewhat strong over the Arabian Sea. However, the accompanying precipitation distribution, Fig. 1b, reveals that precipitation over the subcontinent is underestimated as the model tends to simulate the ocean-mode of the monsoon. The rainfall underestimate over the subcontinent is associated with a Somali jet that is influenced by dry-air advection from the Saudi peninsula, which dilutes the moisture supply through the addition of dry air. Analogously, in the ECMWF model, dry-air advection from the north, and a weak Somali jet north of 12^{o}N, serve to limit the moisture supply through the addition of hot-dry air and reduced evaporation respectively. As a result, the 2mm day^{-1} rainfall contour is displaced eastward relative to the observations. GLA is run at coarser horizontal resolution, and hence the regional features are smoother. Over northern India the model is drier than observed as a consequence of overly strong westerlies from the Thar desert. As with the CCC model, the SNG2 model preferentially rains

near the equator, and exhibits a dry bias over the subcontinent which is associated with strong westerlies from continental Africa and the Saudi peninsula. These biases are characteristic of many of the simulations. Additionally, there is some tendency for a weak Somali jet to be associated with an underestimation of rainfall over the subcontinent. CSU, DERF, UCLA, and UIUC tend to locate the Somali jet just north of the equator and consequently the majority of rainfall occurs over the Indian Ocean to the south of the subcontinent. It is of interest that the CSU and UIUC models share a common lineage with the UCLA model, particularly with regard to boundary layer formulation and numerics. The systematic error in these models does not appear to be resolution related, as the GLA model, which also has a horizontal resolution of 4^0 latitude x 5^0 longitude is able to capture the climatological and interannual rainfall and low-level flow features of the summer monsoon with fidelity (Figs. 1d and i, Figs. 3d and i).

Examination of five additional AMIP integrations with the ECWMF model, run with different initial conditions, exhibit the same biases as seen in Figs. 1c and 1h, indicating that these are robust systematic errors of this model formulation, and hence that a single 10-year simulation is adequate to characterize this model's ability to represent seasonal mean climatological characteristics over this region. Similar results were also found for the SNG2 realizations.

Examination of the 10-year JJAS averaged precipitation and low-level flow climatologies from the ensemble of AMIP integrations suggest that while it is necessary to simulate the large-scale flow in order to obtain a good monsoon precipitation distribution, other regional scale phenomena such as dry-air advection from the northwest and the Saudi peninsula, and the behavior of the trough in the Bay of Bengal play important roles as mechanisms in moderating monsoon precipitation on seasonal time scales. Examination of these various regional attributes in the 10-year climatologies may aid in delineating those models that may have more success at properly simulating the observed interannual variations.

b. Monsoon extremes

1987 and 1988 were El Niño and La Niña years respectively. During the monsoon season the 1988 the tropical Pacific Ocean SSTs were colder than those in 1987 by upwards of 2^0C, with maximum differences reaching 4.5^0C (Fig. 2a). These SSTs were associated with a substantial modulation of the tropical flow and anomalous precipitation over many regions of the globe. The JJAS merged MSU/rainguage data set, given in Fig. 3a, indicates a large-scale enhancement of precipitation over the summer monsoon region in 1988 relative to 1987. The GEOS Precipitation Index (GPI, Janowiak and Arkin

1991) satellite rainfall estimates also exhibit a similar pattern of rainfall enhancement, but over the ocean but it extends further to the southwest of India and the magnitude of the anomalies differ. This is consistent with the Spencer (1993) MSU/GPI intercomparison in which the pattern of large-scale El Niño/La Niña differences are consistent with the caveat that substantial magnitude differences exist locally.

Examination of the low-level flow anomalies at 850hPa from ECMWF analyses (Fig. 3f) indicate that there were several features that contributed to the enhanced precipitation over the Indian subcontinent, the Arabian Sea and the tropical Indian Ocean (Fig.3a). The enhancement of the Somali jet, in conjunction with the presence of low-level equatorial easterlies are associated with convergence and enhanced precipitation over the southern portion of the subcontinent and over the ocean. That the analyzed wind differences are dynamically consistent with the satellite derived precipitation anomalies over this region is comforting since the two data sets are completely independent. Additionally, southeasterly anomalies over the Bay of Bengal strongly suggest that interannual changes in the behavior of the monsoon trough, and suppression of dry-air advection from the north affected the distribution of precipitation over the northern subcontinent.

Table 1 indicates the ability of the models to simulate the enhancement of JJAS rainfall over the Indian subcontinent (area-weighted land only, based on each models land/sea mask) in 1988 relative to 1987, and the afore-mentioned low-level flow anomalies. In general, the models exhibited subsets of these features. Most models simulated an enhanced Somali jet to some degree, but clearly such an increase in the low-level flow did not guarantee enhanced precipitation over the subcontinent (or the ocean). To varying extents, southeasterly anomalies over the Bay of Bengal and the continent were also simulated. Those models that have been successful in simulating the enhanced precipitation over the subcontinent exhibit difficulty in simulating the spatial characteristics of the signal with fidelity.

1988-1987 JJAS differences of precipitation and 850hPa winds for the models whose climatologies we discussed in Fig. 1 are presented in Fig. 3. For CCC, Figs. 3b and 3g, decreased rainfall over the subcontinent is associated with weakened westerly flow over the subcontinent and anticyclonic anomalies in the Arabian Sea. For the ECMWF simulation, Fig. 3c and 3h, the enhanced precipitation over the Indian subcontinent arises as a consequence of southeasterly anomalies over the Bay of Bengal that extends over the Indian subcontinent. These anomalies are indicative of monsoon trough displacements and suppressed dry-air advection, the latter of which tended to be too strong in the climatology. In the GLA simulation a decrease in the strength of the westerlies from the Thar desert region is associated with enhanced precipitation over northern India, while

Table 1: The ability of the available AMIP models to qualitatively simulate the enhanced precipitation and 850hPa flow anomalies during JJAS 1988 relative to 1987 is indicated. (+) indicates some ability to simulate the observed characteristics; (-) indicates that the simulated anomalies are in opposition to those observed, and lack of a symbol indicates that a model failed to simulate a given feature. Those models that qualitatively simulated the all-India rainfall index/SST lag 0 anti-correlation are shaded.

Model	1988-1987 Increased all-India Rainfall	Enhanced Somali Jet	Low-level Equatorial Easterlies	Bay of Bengal South-easterlies	Suppressed Dry-Air Advection	Rainfall/ ENSO SST Teleconnection
Observations	+	+	+	+	+	+
BMRC	+	+			+	+
CCC	-	-	-	+		-
CNRM	+		-	+	+	-
COLA	-	-		-		-
CSIRO	+	+	-	+		+
CSU	+	+	-	-		+
DNM	-	-	-	-		-
ECMWF	+			+	+	+
GFDL	+	+	-	-	+	+
GFDL/DERF	-	+		-	-	-
GISS	+	+		+	-	+
GLA	+	+	+	-	+	+
GSFC/GEOS	+	+	-	-	+	+
IAP	+	+	-	+	+	+
JMA	-		-	+		-
LMD	+	-	-	+	+	+
LMD6	+	+	-	-	+	+
MGO	+	-	+		+	+
MPI	-	+	-	-	-	-
MRI	+	+	-	+	+	+
NCAR	-	+	-	-		-
NMC	+(.16σ)	-		-	+	-
NRL	+	-		+		+
RPN	-	-	-	-	-	-
SUNYA	+(.11σ)	+		-	+	-
SUNYA/NCAR	+					+
SNG2	-					-
UCLA	-	+	-	-		-
UGAMP	+	-	-	+		+
UIUC	+	+		-		-
UKMO	+	-			+	+
YONU	+	+		-	+	-

that to the south is associated with an enhanced Somali jet. GLA simulates a tendency for equatorial Indian Ocean easterlies which forms a region of anomalous convergence and enhanced rainfall in the western Indian Ocean that is qualitatively consistent with observations (particularly the GPI anomalies (not shown)). The SNG2E4 simulation results in drier conditions over India in 1988 relative to 1987. This condition tends to be associated with a suppressed Somali jet. The enhanced rainfall to the south of the subcontinent near the equator is associated with northerly low-level anomalies that are convergent with respect to the climatology in that region. By far the dominant signal in this model occurs in the vicinity of East Asia, with strongly divergent anomalies in the vicinity of Burma and convergent anomalies over China.

In an effort to ascertain the robustness of a model's response to the prescribed sea-surface temperatures, the 1988-1987 anomalies from the five additional ECMWF and four additional SNG2 AMIP initial condition sensitivity simulations have been examined. As indicated in Fig. 4 for the ECMWF simulations, the spatial patterns of the precipitation anomalies are qualitatively similar in the vicinity of the Indian subcontinent, wetter during the summer of 1988 than 1987 in association with southwesterly anomalies at 850hPa in the Bay of Bengal and suppressed dry-air advection to the north (not shown for all the realizations but all similar to that presented in Fig. 3h). For this model, this result suggests that wet or dry tendencies over the Indian subcontinent are predictable, but not the absolute magnitudes and spatial distribution of the anomalies. Brankovic et al. (1994) also found substantial intraensemble spread associated with the summer monsoon rainfall in a three member set of seasonal length integrations using observed initial conditions for JJA 1987 and 1988 using a similar version of the ECMWF model. On the otherhand, the SNG2 initial condition realizations are less robust at reproducing the observed rainfall enhancement over the subcontinent, as seen in Fig. 5. In fact, over large regions, neither the sign or the spatial distribution of the anomalies exhibited any coherence among these realizations.This suggests that as in numerical weather prediction (NWP), multiple realizations are required to assess the robustness of a signal in a given model. A similar conclusion was found in earlier MONEG studies (WMO 1992, 1993) in which 1987 and 1988 seasonal length simulations were initialized by observed conditions from successive days.

The simplest hypothesis one can make regarding the robustness of the rainfall response in the ECMWF model versus the SNG2 model is that the ability to represent such tendencies is related to the fidelity with which a model represents the climatological rainfall distribution. This is supported by the work of Shukla and Fennessy (1994) with the Center for Ocean-Land-Atmosphere Studies (COLA) GCM. As noted in Section 4a

and seen in Figs. 1c and 1e, the ECMWF model better represents the spatial distribution of rainfall (although it tends to be too dry) in the vicinity of the subcontinent than the SNG2 model. A more quantitative analysis of the importance of simulating a good climatology will be presented in Section 4d.

c. *Variations during the period 1979-88*

The June-July-August-September (JJAS) averaged (land only) area-weighted all-India rainfall indices and the verification data (heavy black line, Parthasarathy et al. 1992) for the AMIP decade are presented in Fig. 6a. For each model the rainfall index has been normalized by removing the mean and dividing by the standard deviation in order to account for intermodel biases in the mean and variance as discussed in Section 3a. Overall, the totality of indices exhibit little or no coherence among the simulations in representing the observed interannual variations of Indian monsoon rainfall, even during 1987 and 1988 when the large SST anomalies associated with El Niño and La Niña (Fig. 2a) provided a substantial perturbation to the tropical flow.

Alternatively, we can consider the monsoon from a dynamical point of view through the evaluation of a wind shear index, akin to that described by Webster and Yang (1992), and calculate the 850-200hPa difference of the zonal wind, averaged over the region 40°E-100°E, 0-25°N. The dynamical variability of the monsoon flow exhibits more coherence (Fig. 7a) than the rainfall index. From 1983 onwards the behavior of the NMC and ECMWF analyzed wind shear indices are comparable (not shown). Acknowledging the shortcomings of dealing with NWP analyses due to changing models and initialization/assimilation procedures, we see that the dynamical index is a much less stringent means of verifying interannual monsoon fluctuations. The ensemble of models show marked agreement with the analyses in their behavior during 1986-88, with increased shear (stronger Somali jet and enhanced upper level easterly flow) in 1988 relative to 1987 consistent with Webster and Yang (1992). The suite of AMIP simulations also exhibit coherent behavior during the early 1980's. Ju and Slingo (1995) used a similar dynamical criteria in an analysis of the U.K. Universities Global Atmospheric Modelling Programme (UGAMP) AMIP simulation. While the UGAMP model exhibited substantial skill at simulating the dynamical/ENSO relationship described above, this broad-scale measure of monsoon circulation and the all-India rainfall index were not well correlated, which is consistent with the observational study of Joseph et al. (1994), and the lack of correspondence between the rainfall and dynamical indices presented in Figs. 6a and 7a.

A question of interest is: How can we objectively classify the performance of the models in an effort to ascertain if some underlying order is present in their ability to rep-

resent the interannual variations? While the afore-mentioned case study (Section 4b) is useful for diagnosing individual events, the ability of the models to simulate the statistics of the variability during the AMIP decade through teleconnection analysis is of interest. Given that all of the simulations have used the same SST data set (although transformed to the horizontal grid specific to a given model) we can correlate a models rainfall index with the SST as a measure of a model's ability to correctly respond to the imposed surface forcing. Contemporaneous correlations of the observed all-India rainfall and the wind shear indices with the AMIP SSTs are presented in Figs. 6b and 7b. These are the verification data against which we may compare the simulated teleconnection patterns. Given the few degrees of freedom, eight (does not account for a possible reduction in the number of degrees of freedom due to serial correlation), we have chosen to preserve the spatial information of the correlations, even where it falls below the 95% confidence level ($|r|<0.63$). Both observed indices exhibit a pronounced ENSO teleconnection relationship with the SSTs. Enhanced (decreased) precipitation and wind shear occurs when the SST in the central and eastern tropical Pacific Ocean is below (above) normal. Bounding this region is a u-shaped envelope of positive correlation that extends from the western tropical Pacific into the extratropics of each hemisphere. A major point of importance is that these teleconnection patterns are not peculiar to the 1979-88 decade. Rather, the Indian rainfall/ENSO teleconnection is a robust feature of the ocean-atmosphere system that is found when longer periods of record are analyzed (Bhalme et al. 1983, Rasmusson and Carpenter 1983, Barnett 1984, Parthasarathy and Pant 1984), and as such is a fundamental statistic that models should endeavor to represent.

The models that have qualitatively represented the observed rainfall/ENSO SST teleconnection pattern in Fig. 6b are shown in Fig. 6c. This reduced set exhibits some underlying order in the models ability to simulate extremes of monsoon variability, especially during the last portion of the decade in conjunction with the El Niño and La Niña conditions of 1987 and 1988. In Table 1, these models are indicated in the last column with a "+" sign, and the model row has been shaded. Every model that simulated this teleconnection also simulated the 1988 rainfall increase relative to 1987. In no instance did a model fail to simulate the rainfall increase when it produced the proper teleconnection pattern. However, four models produced a relative rainfall increase although they were unable to simulate the proper teleconnection pattern. In the case of CNRM, NMC and SUNYA, the 1987 rainfall was already 0.5 standard deviations or more above normal, and the 1988 increase was only about 0.1 standard deviations relative to 1987, not a substantial change. In the case of UIUC, the proper teleconnection pattern in the central and eastern Pacific was interrupted by a region of opposing correlation. The model

did however correctly simulate a region of positive correlation extending from the western Pacific into the northern extratropics. The work of Ju and Slingo (1995) suggests that convection in this region modulates the monsoon on interannual time scales based on their diagnosis of the Indian monsoon in the UGAMP simulation. Thus, sole emphasis on the Indian monsoon rainfall link to the central and eastern tropical Pacific SSTs should not be made.

The robustness of the ECMWF model at simulating the observed interannual rainfall variability is shown in Fig. 6e. All of the realizations captured the relative increase in 1988 with respect to 1987, however as noted previously in Fig. 4 intraensemble spread is readily apparent. The rainfall/SST teleconnection patterns of the members of the ensemble have also been evaluated. Five of six ECMWF initial condition realizations produced an ENSO teleconnection pattern in the Pacific Ocean (Fig. 8). One realization, (EC9201), failed to properly capture the anti-correlation in the eastern tropical Pacific, and it had a more diffuse pattern in the central Pacific. It did however capture the positive correlation extending from the western Pacific into the northern extratropics, as did the UIUC model discussed above, and it did capture the enhanced rainfall in 1988 relative to 1987 (Figs. 4 and 6e).

Some models actually produced a teleconnection relationship inverse to that observed, as indicated by the "-" sign in the last column of Table 1. That is, these latter models responded incorrectly to the SST forcing, having a positive correlation between the all-India precipitation and SST in the tropical central and eastern Pacific, and a negative correlation with the surrounding tropical/extratropical SSTs. For example, this is the case for three of five SNG2 initial condition realizations (Fig. 9; SNG2E2, SNG2E4, SNG2E5), and as such the ensembles fail to robustly capture the observed rainfall anomalies (Figs. 5 and 6f). These findings suggest that this model is of limited use in the study of interannual Indian monsoon studies. Liang et al. (1996) indicate that the SNG2 convective parametrization fails to deposit the latent heat release at "a sufficiently high altitude...which may explain the absence of robust and realistic wind field responses over the Eurasian sector" during the course of 1982/83 and 1986/87 ENSO events. In this instance a shortcoming in the physics is such that the internal variability becomes the dominant influence. For a given model it is not clear if shortcomings in model physics or excessive internal variability are at the heart of the problem unless an in depth diagnosis is performed, such as that carried out by Rowell et al. (1995) with the UKMO model. The lack of a robust response by the SNG2 realizations also indicates that simulation of a "proper" teleconnection pattern by a single realization may not be indicative of the robustness of a given model to simulate observed interannual variability, and as suggested

earlier based on the 1987/88 case study, multiple realizations are required to ascertain robustness.

Although 1982 and 1983 were also dry and wet years as indicated by the observed all-India rainfall index (Fig. 6a), analogous to 1987 and 1988, the coherency exhibited by the reduced set (Fig. 6c) in the rainfall anomaly tendency from 1987 to 1988 is not found during 1982 and 1983. This is likely to be related to several factors including the magnitude of the boundary forcing. The clear ENSO pattern seen in the 1988 - 1987 anomalies (Fig. 2a) is absent in the 1983 - 1982 anomalies (Fig. 2b). In the 1983 - 1982 SST difference the cold anomalies in the tropical Pacific Ocean failed to extend to the South American coast and they never exceeded 2°C, while the 1988 - 1987 cold anomalies exceeded 2°C and reached a maximum of nearly 4.5°C near 120°W. Additionally, in the 1983 - 1982 anomalies, eastern Pacific warming in excess of 2°C occurred near the west coast of South America. Either the models lack the necessary sensitivity for the Indian monsoon precipitation to respond to the weaker and less coherent 1983 and 1982 SST differences, or other less well understood controlling factors, such as Tibetan snowcover (Hahn and Shukla 1976, Dickson 1984, Barnett et al. 1989), soil moisture (Meehl 1994a) or extratropical influences (Meehl 1994b) may play a significant role in modulating the interannual variations of the Indian monsoon. Also, it is possible that the rainfall differences are not very predictable because of internal chaotic dynamics associated with intraseasonal monsoon fluctuations (Palmer 1994).

Using the average Brier scores (Eq. 4) in Table 2, we can quantitatively assess the usefulness of employing the teleconnection stratification as a method of quality control for the all-India rainfall and wind shear indices, and for examining the performance of the two sets of initial condition experiments. As discussed in Section 3b, the Brier score is a method of assessing the ability of a suite of models to simulate observed anomalies. Perfect agreement with observations would yield a Brier score of 0.0, while a score of 0.5 would be expected from climatology. For the rainfall indices of the different models, the reduced set that passed the rainfall/SST teleconnection criterion (Fig. 6c) is in best agreement with observations in that they exhibit the smallest Brier score. The models that were unable to simulate the rainfall/SST teleconnection (Fig. 6d) produced a Brier score equivalent to that expected from climatology. The ECMWF realization (Fig. 6e) performed better than the reduced set while the SNG2 model, which exhibited greater sensitivity to the initial conditions than the ECMWF model has a less satisfactory Brier score.

The Brier scores for the wind shear indices were calculated for those models that were (Fig. 6c), and were not able (Fig. 6d), to simulate the rainfall/SST teleconnection in

Table 2: Average Brier scores for the departures of all-India rainfall (JJAS), monsoon wind shear (JJAS), Nordeste rainfall (MAM), and Sahel rainfall (JAS) for all AMIP models, those models that qualitatively simulated the lag 0 rainfall index/SST teleconnection, those that failed to simulate the lag 0 rainfall index/SST teleconnection, and the ECMWF and the SUNYA/NCAR Genesis 2 initial condition sensitivity integrations. Brier scores may range from 0.0 (perfect agreement with observations) to 2.0 (total disagreement with observations). A Brier score of 0.5 would be expected from climatology. The number of models analyzed in each category is given in parentheses. Only years in which the departure of the observed index exceeded +/- 0.25 standard deviations were included in the analysis. The years that did not meet this criterion are given in brackets under the index heading.

	India Rainfall [1984]	Monsoon Windshear [1982]	Sahel Rainfall [1985, 1986]	Nordeste Rainfall [1981, 1987]
All	.35 (32)	.22 (32)	.53 (32)	.15 (32)
Agree	.34 (17)	.17 (17)	.41 (16)	.09 (26)
Disagree	.50 (15)	.30 (15)	.74 (16)	.65 (6)
ECMWF	.26 (6)	.60 (6)	.45 (6)	.01 (6)
SNG2	.37 (5)	.52 (5)	.64 (5)	.38 (5)

Fig. 6b (thus the same models were used for the all-India rainfall and the wind shear "Agree" and "Disagree" categories in Table 2). The lower Brier scores for the wind shear relative to the rainfall confirms our original supposition that the dynamical signature of the monsoon exhibits greater predictability than the rainfall. The scores also indicate that the models that best represent the Indian monsoon precipitation variations also tend to better represent the monsoon wind shear index. That this is not always the case is evidenced by the ECMWF realizations which have a wind shear Brier score that indicates the model performs worse than climatology in this respect. As for the rainfall, the wind shear from SNG2 realizations exhibit greater scatter, and hence Brier scores near climatology, than those produced by the ECMWF realizations.

The ability of the models to simulate the same temporal sequence of events is given in Table 3, the Reproducibility. As discussed in Section 3c, the Reproducibility is a model-model intercomparison, and is a measure of the temporal coherence of a suite of simulations. In the hypothetical case when a suite of simulations have the same exact temporal sequence of events, the Reproducibility would be infinite. For the Indian monsoon rainfall, the Reproducibility is in all cases less than 1, which indicates difficulty in discerning the signal from the noise. That the Reproducibility increases for the reduced set of mod-

Table 3: Reproducibility of the normalized all-India rainfall (JJAS), monsoon wind shear (JJAS), Nordeste rainfall (MAM), and Sahel rainfall (JAS) for all AMIP models, for those models that qualitatively simulated the lag 0 rainfall index/SST teleconnection, those models that did not simulate the lag 0 rainfall index/SST teleconnection, and the ECMWF and SUNYA/NCAR Genesis 2 initial condition sensitivity integrations.

	India Rainfall	Monsoon Windshear	Sahel Rainfall	Nordeste Rainfall
All	.19	.89	.16	.68
Agree	.49	1.03	.53	1.45
Disagree	.44	.80	.14	.22
ECMWF	.81	2.78	2.38	9.09
SNG2	.21	1.18	.22	2.07

els that were able to simulate the rainfall/SST teleconnection pattern again demonstrates the usefulness of using the teleconnectivity as a quality control procedure. For the monsoon wind shear, the Reproducibility is greater than the rainfall in all categories indicating that the models give a more robust dynamical response to the imposed SSTs. Consistent with Figs. 4-9, the ECMWF model exhibits greater Reproducibility than the SNG2 model. However, caution in using this score alone is warranted as indicated for the case of the monsoon wind shear for the ECMWF model. While its Reproducibility is well in excess of 1, its Brier score indicates poor agreement with observations.This indicates the model is robust at reproducing a poor wind shear index. However with regard to the Indian monsoon rainfall, the ECMWF model exhibits the largest Reproducibility and the best Brier score. Hence, consideration of the Reproducibility in conjunction with the Brier score is important.

d. Climatological Rainfall versus Interannual Variability

In Section 4b we hypothesized that a good rainfall climatology and proper simulation of interannual variability are associated. This was based upon the better representation of the JJAS rainfall climatology in the vicinity of India, and the more coherent 1988 - 1987 response in the ECMWF simulations relative to the SNG2 realizations. To further investigate this hypothesis, we have area-weight interpolated all of the model JJAS rainfall climatologies to the same horizontal grid as the observed MSU/rain gauge verification data (4° latitude x 5° longitude). The observed data and the average climatology of the complete suite of AMIP simulations are given in Figs. 10a and b. We have

then performed pattern correlations for the two regions in Fig. 10a as a method of quantifying the ability of the "average" model to simulate the observed spatial distribution of rainfall. The "average" model exhibits a pattern correlation of approximately 0.6 for the regions selected. The "average" model fails to properly represent the rainfall maxima associated with the western Ghats, it is too far south, and tends to simulate too much rainfall over the equatorial Indian Ocean. Additionally, there is a dry bias over northwest India. Figure 10c shows the average rainfall climatology of those models that passed the observed rainfall/SST teleconnection criterion (Fig. 6c), and that from those models that were unable to simulate the observed teleconnection (Fig. 6d) is presented in Fig. 10d. The models that passed the observed rainfall/SST teleconnection criterion have substantially larger pattern correlations with respect to the observations than those models that didn't pass this quality control criterion. For the smaller region, the pattern correlation improvement is even more demonstrative (0.68 versus 0.47) indicating that the quality controlled subset exhibits the greatest fidelity at representing the regional scale rainfall distribution, principally in representing the rainfall maxima along the west coast of India. This subset also has less of a dry bias over northwestern India, while the latter subset preferentially rains over the equatorial Indian Ocean at the expense of the subcontinent, and has a much poorer pattern correlation with respect to the "average" model in Fig. 10b.These conclusions are also borne out if another rainfall climatology is employed (e.g. Jaeger 1983).

5. SAHEL RAINFALL

a. 1979-88 Climatologies

The Sahel is located at the northern flank of the tropical African boreal summer rainfall belt. Over this region, the peak rainy season occurs during July-August-September (JAS) as the Inter-Tropical Convergence Zone (ITCZ) attains its most northern position, near 15°N (in the vicinity of Sudan and points east it is located further south, near 10°N) due to the seasonally enhanced surface solar heating over the deserts of northern Africa. Hastenrath (1988) and Lamb and Peppler (1991) review the literature regarding the governing influences and variability of Sahel precipitation.

Since the Sahel and vicinity were in a prolonged drought phase during the AMIP decade we have chosen to show the JAS 1979-1988 MSU/raingauge data (Fig. 11a; JAS raingauge data was not available for the full 10 years at some grid points and data was considered to be missing if less than 7 years were available from which to construct the time mean field) rather than observed data based on a long term climatology. During the

AMIP decade the rainfall amounts over this region are in fact reduced relative to the Jaeger (1983) and the Legates and Willmott (1990) data sets. This low frequency modulation appears to be related to interhemispheric changes in SST in the Atlantic Ocean (Folland et al. 1986). The ability of GCMs to simulate the observed interdecadal variations of Sahel rainfall is being studied in multi-decadal simulations forced with the Global Ice and Sea-Surface Temperature (GISST) data set assembled by the UKMO Hadley Centre. The low-level flow, based on ECMWF analyses (Fig. 11f), into the rainbelt is from the southwest (Critchfield 1983), and the dominant moisture source tends to originate from south of the equator (Hastenrath 1988). The cross-equatorial southwesterly flow is the dominant influence in the vicinity of the Gulf of Guinea, while over eastern Africa, moisture from the Indian Ocean may exert substantial influence (Palmer 1986). The rainfall maximum over western Africa may be influenced by moisture from the northern tropics as hinted by the westerly flow over west Africa near 9°N.

Figure 11 also shows the JAS climatological rainfall and 850hPa flow from some of the AMIP simulations. Unlike that observed, DNM has excessively strong southwesterlies, >4m s^{-1}, that bring moisture from the northern tropics deep into the interior of Africa. The convergence zone is incorrectly located near 25°N, and the rainfall extends deep into what should be the Sahara Desert. On the other hand, all six of the ECMWF realizations, of which two are shown (Figs. 10c-d), exhibit characteristics that are similar to the observed and analyzed data. They capture three main centers of rainfall (seen in the observations if more contours are used) although the rainfall is underestimated over much of the region. The 850hPa cross-equatorial flow (Figs. 11h-i) is readily apparent, but the weak onshore westerlies near 9°N noticed in the ECMWF analyses are absent. The UKMO simulation exhibits a smoother rainfall distribution (Fig. 11e), but the overall magnitude is more consistent with observations than that produced by the ECMWF model. The precipitation in these latter two models is also confined latitudinally relative to the observations. The UKMO 850hPa flow (Fig. 11j) suggests that the moisture for at least the western half of the Sahel has its origin in the northern tropics. This may however be misleading since the wind data are based on data from throughout the course of the day and averaged over the month. To ascertain the importance of this "potential" moisture flux would require data to analyze the diurnal cycle since the rainfall maxima tends to occur around the time of maximum solar heating (Rowell 1995, personal communication). Westerly flow through the Gulf of Guinea and southwesterlies to the south are the dominant influences further east.

While most of the models produce a reasonable rainfall climatology in the vicinity of the ITCZ over the African sector during boreal summer, the low-level flow strongly

suggests that a wide-range of possible moisture flux scenarios may give rise to such a rainfall pattern. How realistic this range of scenarios is has yet to be determined.

b. Extreme Events

As with the Indian monsoon, 1987 and 1988 were extreme years with respect precipitation accumulation during the AMIP decade. Sub-Saharan Africa experienced a relative enhancement while to the south concomitant rainfall anomalies of opposite sign are noticed (Fig. 12a). Similar dipole patterns have been observed on prior occasions (Hooky 1970, Tanaka et al. 1975, Lamb 1978a and Motha et al. 1980). The 850hPa wind anomalies are dominated by westerlies in the vicinity of 10°S-15°N (Fig. 12f). Over an extensive region the magnitude of these anomalies are in excess of the climatological wind speeds indicating that substantial modulation of the tropical circulation occurs in tandem with the rainfall displacement. For the model simulations, including those presented in Fig. 11, considerable uncertainty in the simulation of the westerly anomalies exists, particularly over the eastern Atlantic and western Africa. In those simulations with weak or poorly defined westerly anomalies there is a tendency for lack of a robust rainfall signal, particularly over the western Sahel. This implies that the low-level moisture flux from the Atlantic and the Gulf of Guinea plays an important role in modulating the Sahel rainfall variations in this case study. Using a version of the Goddard Institute for Space Studies (GISS) GCM, Druyan and Hastenrath (1991) found that reduced low-level moisture inflow from the Gulf of Guinea was associated with drier Sahel conditions. Druyan and Koster (1989) also implicated enhanced local recycling through continental evaporation to be associated with enhanced Sahel rainfall. Moisture from the Indian Ocean was not implicated in the Sahel rainfall variations in these latter two GCM studies or in the Cadet and Nnoli (1987) analysis of First GARP (Global Atmospheric Research Program) Global Experiment (FGGE) data. The AMIP model results presented in Fig. 12 appear to be consistent with this finding. The influence of the low-level flow from the Atlantic Ocean is readily visible in the two ECMWF simulations shown in Figs. 12c-d. These are the best and worst of the six ECMWF initial condition realizations for this Sahel case study, and they suggest a sensitivity to internal variability. Conversely, in numerical experiments using composite SST anomalies based on wet versus dry Sahel years, Palmer (1986) found that anomalies in rainfall "across the Atlantic and into the extreme western Sahel are extremely reproducible." However, examination of the composite SST anomalies used by Palmer (1986) reveals the presence of a dipole pattern of SST that straddles the usual location of the ITCZ in the Atlantic that is not present in the JAS 1988-1987 difference pattern (Fig. 13). The dipole in the Palmer (1986) study affected the strength

of the Hadley circulation and the flux of moisture into the ITCZ. Such a dipole is also seen in the Folland et al. (1991) correlation of Sahel rainfall and SST for the period 1901-1986 (not shown). However, it is absent from the interannual Sahel rainfall/SST correlation for the AMIP decade (Fig. 14b). In the former case the southern tropical Atlantic correlation is the same sign as that in the central and eastern tropical Pacific, while for the AMIP decade the correlation (and the 1988 - 1987 SST anomalies) to the southwest of the Gulf of Guinea are reversed relative to the tropical Pacific. Thus, the SSTs are such that thermally direct circulation anomalies in the Atlantic are not preferred which might otherwise be conducive to northward displacement of the ITCZ in 1988 relative to 1987. Rather, the remote forcing of tropical Pacific and Indian Ocean are left to exert their influence on this region (through modification of the circulation) with less effect, and hence allow a greater sensitivity to internally generated atmospheric fluctuations.

c. *Variations during the period 1979-88*

While it is acknowledged that there is some regionality to variations in Sahel rainfall (Nicholson and Entekhabi 1986), for the purpose of model intercomparison of interannual rainfall variations we define a single land only Sahel rainfall index based on the region 15°W-38°E, 12°N-18°N. As noted earlier, the Sahel was in the midst of a prolonged drought throughout the AMIP decade, so the observed rainfall index, based on the station data of Sharon Nicholson through 1984, with subsequent updates (Hulme 1994) provided by the Hadley Centre (Rowell and Ward 1991, personal communication), has been renormalized for the 1979-88 decade. The indices of all of the AMIP runs are given in Fig. 14a, and as with the Indian monsoon rainfall index, consistency among the simulations is lacking. As an ensemble, all of the models exhibit less skill than climatology in representing the rainfall variations over the Sahel as indicated by their average Brier score in Table 2, and the Reproducibility is less than that for all-India rainfall for the ensemble of models as seen in Table 3. Rowell et al. (1995) demonstrate that modelling the Sahel region is problematic.

Teleconnections of the Sahel rainfall variations to SST in the Atlantic, Pacific and Indian Oceans has been discussed in Lamb (1978b), Folland et al. (1986), Lough (1986), Palmer (1986), Nicholson and Entekhabi (1986), Hastenrath (1988), Folland et al. (1991). As alluded in the previous section, the Atlantic teleconnection exhibits a higher degree of non-stationarity than either that over the Pacific or Indian Ocean during the AMIP decade, and it is not realized as coherently as in records of longer duration. In fact none of the models was able to simulate the tropical Atlantic teleconnection pattern in the Atlantic Ocean similar to that in Fig. 14b. Hence, the model stratification teleconnection

criterion is based upon the ability of a model to generate the ENSO correlations over the Pacific, and the correlations in the vicinity of the western Indian Ocean. These models have been retained in Fig. 14c, and their rainfall indices exhibit some common features, particularly during the transition periods into and out of the 1982/83 and 1986/87 El Niños. As indicated in Table 2, this teleconnection stratification results in an improved skill score relative to all models and to those that did not exhibit teleconnectivity similar to observations (Fig. 14d), but their skill at simulating the Sahel rainfall variations was inferior to their ability to simulate the fluctuations associated with the Indian monsoon.Tables 2 and 3 indicate that the ECMWF model (marginally) beats climatology in representing the observed interannual variability in Sahel rainfall, and its Reproducibility is high suggesting that this model is skillful at representing interannual Sahel rainfall variations, particularly those years associated with extremes of the ENSO phenomenon. Also, The data in Tables 1 and 2 also confirm what can be seen in Figs. 14e and f, that the ECMWF model is more robust in its simulation of Sahel rainfall variations than is the SNG2 model.

6. NORDESTE RAINFALL

a. *1979-88 Climatologies*

Northeast Brazil lies under influence of each of the semi-permanent anticyclones in the Atlantic Ocean. The seasonality of this interplay is such that the majority of Nordeste rainfall occurs during the austral autumn when the ITCZ makes its southernmost excursion. Chu (1991) presents a synopsis of the general circulation and interannual variability of Nordeste rainfall. The location of the rainfall maxima (Fig. 15a; the MAM raingauge data was not available for the full 10 years at some grid points, particularly in the vicinity of Africa, and at a few points to the north and south of the main rainbelt over South America, and data was considered to be missing if less than 7 years were available from which to construct the time mean field) is closely linked to the axis of confluence as seen in the low-level flow (Fig. 15f), with the Nordeste located near the southern flank of the ITCZ. Typically, the models produced rainfall maxima in the vicinity of the Nordeste region, with the intensity of the onshore flow along the east coast of South America exhibiting the most variability (Figs. 15g-j). Uncertainty is also associated with the orientation and magnitude of the rainfall in the ITCZ (Fig. 15b-e). Some models simulated rainfall rates <2 mm day^{-1} over the eastern Atlantic Ocean (e.g. Fig. 15d). In such cases the southeasterly trades were too weak in this vicinity (Fig. 15i). The ECWMF initial condition realizations rainfall climatologies exhibited slight differences in eastern Atlan-

tic portion of the ITCZ (on the order of 1mm day^{-1}) and the South Atlantic Convergence Zone (not shown), but were robust in the vicinity of Nordeste. Such is the case for the SNG2 initial condition realizations (not shown), which situate the maximum rainfall directly over the Nordeste, too far south relative to the observations.

b. Extreme Events

Since the Nordeste lies near the southern periphery of the ITCZ, displacements of a couple of hundred kilometers in either direction tend to result in either drought or flood over this region. Such ITCZ displacements are sensitive to the north/south gradient of SST in the tropical Atlantic Ocean (Moura and Shukla 1981). Typically, the SST anomalies in the northern tropical Atlantic lag that in the central and eastern tropical Pacific by approximately 3 months during the early portion of the calendar year, while at such time the SST anomalies in the southern tropical Atlantic are usually of the opposite sign. During El Niño (La Niña) the gradient of SST in the tropics is such that a northward (southward) displacement of the ITCZ occurs with the result that the Nordeste experiences drier (wetter) than normal conditions. Such conditions are associated with a strengthened (weakened) Southern Hemisphere anticyclone in the Atlantic that typically occurs during El Niño (La Niña) (Hastenrath and Heller 1977, Markham and McLain 1977, Covey and Hastenrath 1978).

During the AMIP decade, such a north/south SST gradient in the Atlantic, which is on the order of 1.5°C to 2°C, is evident in the difference map of 1984 - 1983 SST (Fig. 16), which also clearly portrays the ENSO signature in the Pacific. This occurs in conjunction with the largest change of Nordeste rainfall during the AMIP decade, with drought in 1983 and flood in 1984. The enhancement of rainfall over the Nordeste region and the deficit to the north in 1984 relative to 1983, as seen in Fig. 17a, is based on the merged MSU/rainguage data. Such dipole patterns of rainfall anomalies have been reported previously (Hastenrath and Heller 1977, Hastenrath et al. 1984, Hastenrath 1988) and are consistent with a displacement of the ITCZ as proposed by Moura and Shukla (1981). In a study of the water vapor flux during extreme years, Rao and Marques (1984) find the dominant moisture source to be from the South Atlantic Ocean, but the large-scale flow (more northerly during wet years) is consistent with the placement of the ITCZ, and in determining whether the flux is convergent or divergent over the Nordeste.

The low-level flow anomalies, Fig. 17f, based on ECMWF analyses, indicate pronounced onshore northerly flow in the vicinity of Guyana and offshore westerly flow to the south near the Nordeste. Aceituno (1988) found such a relationship in his study of Nordeste precipitation and ENSO using the Comprehensive Ocean Atmosphere Data Set

(COADS, Woodruff et al. 1987), and Bruce et al. (1985) noted the presence of enhanced offshore flow near Guyana in March 1983 during the Nordeste drought phase. Similar anomalies were found by Moura and Shukla (1981) in an atmospheric GCM simulation in an early study to diagnose the mechanisms controlling Nordeste rainfall variability in which it was proposed that thermally direct circulation anomalies give rise to the ITCZ displacements which dominate the modulation of Nordeste rainfall. Mechoso et al. (1990) confirmed this scenario in a case study of the 1984, and later, Hameed et al. (1993) found such anomalous circulation and rainfall patterns in a study of Southern Oscillation teleconnections in the tropical Atlantic sector in a coupled ocean-atmosphere model simulation.

Only 3 of 32 models were unable to simulate enhanced rainfall in 1984 relative to 1983, but this arose because these anomalies were displaced too far south. Also, the Nordeste region is quite small with respect to the grid box size of the models, and is here take to encompass gridpoints whose nodes fall in the domain 35°W-42.5°W, 4°S-10°S (This is a slightly larger domain than actually encompassed by the Nordeste to ensure that data from the coarse resolution models would not be based upon one gridpoint). The rainfall and low-level flow anomalies from some of the models are also shown in Fig. 17. The response to the SST forcing tends to be consistent with the observations, although the magnitude and spatial distribution of the anomalies exhibit variability from model to model, though generally they are more consistent than the intermodel variability for the Indian and Sahel monsoon regions.

BMRC, DNM and MGO failed to simulate the enhanced Nordeste precipitation in 1984 relative to 1983. For DNM and MGO the low-level flow anomalies suggest that the water vapor flux over Nordeste is actually divergent since northwesterly anomalies are present to the northwest and to the southeast of Nordeste. In the ECMWF analyses, Fig 17f, southerly anomalies to the south of Nordeste intersect the northwesterly flow from the north indicative of anomalous convergence and enhanced rainfall over Nordeste, and in agreement with the observations of Rao and Marques (1984). In the case of BMRC, the anomalous convergence is displaced just to the south of the Nordeste. Examination of the low-level flow anomalies from the six ECWMF realizations (not shown) also indicate that the anomalous flow from the south of 10°S to be the least reproducible aspect of the simulations over this region in this case study. Not surprisingly, the SNG2 simulations exhibited greater uncertainty in the simulation of anomalies over the Nordeste relative to the ECMWF runs.

c. Variations during the period 1979-88

The variability of March-April-May Nordeste rainfall during the AMIP decade (March-April for the observations; Hastenrath 1992, personal communication) is given in Figure 18a. While there is still substantial spread among the models, there is an indication of more coherent behavior, particularly during 1982-88. This is consistent with the lower all-model Nordeste Brier score in Table 2 and their larger Reproducibility in Table 3 when compared with the Indian and Sahel monsoon rainfall time series. The observed Nordeste rainfall index exhibits a pronounced ENSO teleconnection relationship with the SSTs as noticed in Fig. 18b. Enhanced (decreased) precipitation occurs when the SST in the central and eastern tropical Pacific Ocean is below (above) normal, and it is also significantly related to a dipole SST pattern in the tropical Atlantic Ocean. Such teleconnection relationships abound in the literature (Hastenrath and Heller 1977, Moura and Shukla 1981, Ropelewski and Halpert 1987, Aceituno 1988, Ward et al. 1988, and Sperber and Hameed 1993), hence the patterns presented here are not peculiar to the 1979-88 decade. Through combining the SST signals from the tropical Pacific, the northern tropical Atlantic and the southern tropical Atlantic, Sperber and Hameed (1993) were able to demonstrate that the Nordeste rainfall variations were phase locked with the SST on quasi-biennial, ENSO, and decadal time scales, and this composite SST signal explained approximately 80% of the Nordeste rainfall variability. As demonstrated by the improved Brier score in row 2 of Table 2, and the greater coherence of the model indices (Table 3) for this subset of the data (Fig. 18c), skill improves for the models whose rainfall/SST teleconnection pattern is akin to that observed (Fig. 18b). The signal exceeds the noise by approximately 45%, and the Brier score is <0.1 indicating substantial skill at simulating the observed anomalies of Nordeste rainfall (even in non-ENSO years). In the case of the ECMWF model realizations (Fig. 18e), the Reproducibility is in excess of 9.0, and the Brier score approaches zero; indicative of near perfect Reproducibility among the realizations.Consistent with the results for the other study regions, the SNG2 realizations (Fig. 18f) exhibit greater sensitivity to internal variability than the ECMWF model as reflected in the poorer Brier score and the lower Reproducibility. The models that were unable to simulate the observed rainfall/SST teleconnection pattern (Fig. 18d) exhibited a Brier score worse than climatology, and the noise exceeded the signal by ~4 to 1 as denoted by the Reproducibility.

The BMRC model is one of six that did not meet the teleconnection criterion having failed to properly capture the ENSO SST teleconnection pattern over the Pacific Ocean (Fig. 19b, compare with the observations in Fig. 18b), and it one of three models that did not simulate the 1984 - 1983 rainfall difference. Interestingly, this model exhibits pro-

nounced biennial variations in its Nordeste rainfall index (Fig 19a). Sperber and Hameed (1993) analyzed 35 years of Nordeste rainfall and examined its relationship to SST in the Pacific and Atlantic Oceans. Their analysis indicated that the north-south gradient of SST in the Atlantic exhibited greater power on biennial time scales than on ENSO time scales, whereas the Pacific SSTs were dominated by periods of ~3.3-6 years associated with ENSO. That the BMRC Nordeste rainfall is dominated by biennial times scales is consistent with its simulation of the proper teleconnection in the Atlantic and its failure to realize the longer period modulation of ENSO over the Pacific. This result suggests that the phase-locking interactions found by Sperber and Hameed (1993) are operating in the AMIP simulations. However, due to the length of the AMIP simulations, spectral decomposition of these modes is not possible to evaluate this hypothesis in more detail. Examination of this phenomenon should be possible with the multi-decadal GISST simulations.

7. RESOLUTION, CONVECTIVE CLOSURE AND NUMERICAL SENSITIVITY

While this study develops a method of delineating model performance on interannual time scales, it has not addressed the causes of such differences. In an effort to do so, albeit crudely, we investigate the relationship of the models to successfully simulate the observed rainfall/SST teleconnections with respect to horizontal resolution, convective closure, and numerics. Figure 20 shows the results for the all-India and Sahel rainfall, as the models exhibited the greatest difficulty simulating rainfall over these regions. Since the majority of models were able to simulate the Nordeste rainfall and monsoon windshear indices, they have been excluded from such an analysis. In each panel, the models are arranged from low to high horizontal resolution. Models inclusive of and to the right of CNRM have resolutions ≥T42, at which models begin to resolve tropical synoptic-scale activity, and are henceforth referred to as high resolution models. Models to the left of CNRM will be denoted as low resolution models.

Ignoring the shading for the moment, we note that overall 53% (17/32) of models were able to simulate the observed all-India rainfall/SST teleconnection (Table 1, Table 2 and Fig. 6c). The results with respect to resolution are more revealing, and indicate that only 27% (3/11) high resolution models were successful in simulating the observed teleconnection, while 67% (14/21) of the low resolution models were successful (Fig. 20a). Thus, by an overwhelming majority the low resolution models exhibit superior performance in the simulation of interannual rainfall variations over the Indian subcontinent. This is not to say that low resolution models are necessarily preferable to high resolution

models, as it is unlikely that they are able to resolve and simulate the proper sequence of synoptic scale events that characterize the evolution of the monsoon. Sperber et al. (1994) examined the synoptic scale evolution of the summer monsoon at T21, T42, T63 and T106 in an earlier version of the ECMWF model (cycle 33), and found that only the T106 simulation was able to properly simulate the recurring milestones in the synoptic evolution of the Indian (and East Asian) summer monsoon.

For the Sahel (Fig. 20b), the disparity in performance between the high resolution models and the low resolution models is consistent with the tendency noted above for the all-India rainfall, however it is not as striking. 45% (5/11) of the high resolution models correctly simulated the observed Sahel rainfall/SST teleconnection, and 52% (11/21) of the low resolution models were successful.

With regard to the convective closure, 60% (12/20) of the models that used a buoyancy closure (inclusive of other closure techniques that do not rely upon moisture convergence) were successful at simulating the observed all-India rainfall/SST teleconnection (Fig. 20a), while 42% (5/12) of the moisture convergence models were successful. This suggests that moisture convergence may not be preferable (not taking resolution into account). Examining the convective closure as a function of resolution is instructive. At low resolution, 63% (10/16) of the buoyancy closure models were successful, while 80% (4/5) of the moisture convergence models were successful (suggesting a slight preference of moisture convergence schemes at low resolution). At high resolution, 50% (2/4) of the buoyancy closure models were successful, while only 14% (1/7) moisture convergence models were successful. This latter finding strongly suggests that moisture convergence is not appropriate for resolutions ≥T42.

For Sahel rainfall (Fig. 20b), the convective closure statistics are consistent with those of the all-India rainfall. At low resolution, moisture convergence exhibits a slight advantage relative to buoyancy closure with a 60% (3/5) success rate relative to 50% (8/16) respectively. At high resolution buoyancy closure has a 50% (2/4) success rate relative to 43% (3/7) for moisture convergence. While it may be questionable to conclude that moisture convergence is not appropriate for resolutions ≥T42 based on the results from two regions, Slingo et al. (1996), in their examination of a subset of these integrations, find that intraseasonal activity is best simulated when the convective parametrization is closed on buoyancy rather than moisture convergence, and these models were also demonstrably better at simulating the observed relationship between precipitation and SST. Further evidence is found in a sensitivity study of convective parametrizations using the UGAMP GCM in which Slingo et al. (1994) found more realistic transient activity with a convective scheme that did not employ moisture convergence. Additionally, Nor-

deng (1996) demonstrates improved transient activity in the tropics of the ECMWF model when the convective scheme employs buoyancy closure rather than moisture convergence. As most high resolution models use moisture convergence, the conclusion that high resolution is worse than low resolution is really only suggestive about the way in which resolution and convection interact.

The influence of numerics, gridpoint versus spectral, is explored in Figs. 20c-d. This may be important given the concern of how diabatic tendencies (which are computed in gridpoint space) project onto the dynamics (which are computed in spectral space; Lander 1994). The majority of AMIP entries employ spectral numerics. On a percentage basis however, gridpoint models were 62% (8/13) successful while spectral models were 47% (9/19) successful at simulating the observed all-India rainfall/SST teleconnection (not accounting for resolution). At low resolution the number of spectral models and gridpoint models is approximately equal (11 versus 10 respectively), and their success rates were approximately equal (70% (7/10) and 64% (7/11) respectively). Similar tendencies also occurred for the Sahel rainfall/SST teleconnection. Irrespective of resolution, the gridpoint models were slightly more successful than the spectral models (54% (7/13) and 47% (9/19) respectively). At low resolution the spectral models held the edge in performance with a 60% (6/10) success rate versus a 45% (5/11) success rate for gridpoint models.

At high resolution only two models employed gridpoint numerics, thus comments reading their performance will not be made. For the spectral models, the level of performance that occurs at high resolution is very poor, with the spectral success rates for India and the Sahel being only 22% (2/9) and 33% (3/9) respectively. We don't wish this to be interpreted as evidence for scraping of the use of spectral numerics at high resolution (where it has computational advantages over the gridpoint method until approximately T250), but it suggests an interesting sensitivity study in which the spectral numerics would be converted to gridpoint numerics while keeping the physics unchanged. It should however be kept in mind that the majority of the high resolution spectral models employed a moisture convergence closure criterion in their convection scheme. Given the findings of Slingo et al. (1994), Nordeng (1996) and Slingo et al. (1996) mentioned above, our first priority would be to suggest more sensitivity studies of convective parametrization closure in high resolution models rather than the changing of numerics, which is a much more involved conversion.

8. DISCUSSION AND CONCLUSIONS

The climatologies and interannual variations of Indian and Sahel summer monsoon, Nordeste rainfall and low-level flow have been examined from 32 atmospheric general circulation models that have been run as part of the Atmospheric Model Intercom parison Project using a common set of boundary conditions for the period 1979-88. The use of a regional rainfall index as a means of model verification has proven to be a stringent test of a models ability to simulate interannual variations. Of these three regions, the interannual variability of Nordeste rainfall is the most readily simulated, as indicated by the lowest average Brier score and the greatest Reproducibility, owing to the its intimate link with subtropical Atlantic and Pacific SSTs. That this link is robust, and as such indicates predictability in non-ENSO years, is reflected in the Brier scores for the individual years given in Table 4. The Nordeste Brier scores are among the lowest values found of the indices evaluated, and in no year does the Brier score approach that expected from climatology (0.5). As such, Nordeste is the only region for which long-lead predictions are made using an atmospheric general circulation model (Graham 1993). Statistical/dynamical or purely statistical methods are otherwise used in practice (Hastenrath 1994).

The summer monsoon wind shear indices exhibit similarly low Brier scores, but not for all years. It however, is better simulated in comparison to the all-India rainfall which tends to have larger (poorer) Brier scores. Additionally, those models that best represent the observed all-India rainfall/SST teleconnection tend to better represent the wind shear index. We find that the link between Indian monsoon rainfall and SST is strongest under ENSO conditions, particularly when substantial anomalies in the tropical Pacific Ocean persist during June-September, such as in 1987 and 1988. At other times little or no consensus among the simulations exists with regard to Indian monsoon rainfall, even in the initial condition sensitivity simulations. In the case of the ECMWF initial condition simulations, the 1988-1987 differences showed similar structure with the precipitation enhancement over the subcontinent being associated with reduced dry air advection from the northwest and southeasterly anomalies over the Bay of Bengal, the latter being suggestive of monsoon trough perturbations. While all were wetter over the subcontinent in 1988 relative to 1987, five out of six of ECMWF realizations produced wetter conditions relative to the 1979-1988 climatology. This indicates that this particular model can qualitatively represent relative impacts over this region but not absolute responses to the remote forcing.

Table 4: Brier scores for individual years for the departures of all-India rainfall (JJAS), monsoon wind shear (JJAS), Nordeste rainfall (MAM), and Sahel rainfall (JAS) for all AMIP models for those models that qualitatively simulated the lag 0 rainfall index/SST teleconnection. Brier scores may range from 0.0 (perfect agreement with observations) to 2.0 (total disagreement with observations). A Brier score of 0.5 would be expected from climatology. The number of models analyzed in each category is given in parentheses. Only years in which the departure of the observed index exceeded +/- 0.25 standard deviations were included in the analysis. The years that did not meet this criterion are given in brackets under the index heading, and are left blank in the table.

Year	India Rainfall [1984]	Monsoon Windshear [1982]	Sahel Rainfall [1985, 1986]	Nordeste Rainfall [1981, 1987]
1979	.56	.56	.28	.05
1980	.06	.03	.50	.24
1981	.06	.00	.50	-
1982	.25	-	.78	.19
1983	1.36	.03	.01	.00
1984	-	.06	.78	.05
1985	.44	.25	-	.00
1986	.34	.56	-	.07
1987	.00	.01	.01	-
1988	.01	.06	.38	.11

The Sahel variability has proven the most difficult to simulate, with half of the years having Brier scores as poor, or poorer than expected from climatology. One point of note from Table 4 is that the departures in the La Niña year of 1988 are not as well simulated as those during the El Niño year of 1988. Of course we acknowledge the caveat that this is a very limited time period of data from which to draw conclusions regarding the relative predictability during El Niño versus La Niña years.

Examination of the 10-year mean climatologies from the simulations indicates that regional scale characteristics of the low-level flow can have dramatic consequences on the distribution of precipitation over the monsoon region. For instance, many models simulated a Somali jet that compared well with observations. This is generally assumed to be related to a models ability to properly represent the precipitation along west coast of India. While we have typically found this to be the case in these simulations, the nature of

the low-level flow over Pakistan, Afghanistan and the Saudi peninsula also plays a crucial role. When flow from these regions is excessive, dry hot air is advected into the monsoon region, and this precludes the moisture converge necessary to produce the copious amounts of precipitation associated with the monsoon. This is but one example of the many controlling influences that govern the monsoon which must be modelled adequately if GCMs are to be used as a tool for monsoon prediction. Furthermore, our results indicate that interannual variability is better simulated in models that generate a climatology that is in agreement with observations.

Examination of initial condition sensitivity simulations with two different models indicates that the level of internally generated variability is model specific. As such, multiple realizations are required to assess the ability of a model to robustly respond to the imposed SSTs. Thus, one should not conclude that those models that were able to simulate the various rainfall/SST teleconnections in Figs. 6c, 14c and 18c would respond robustly in a series of initial condition experiments. It is possible that some of these models passed this criterion by chance (as was the case for the SNG2 realizations for the all-India and Sahel rainfall), and that an even smaller subset are actually simulating the observed interannual variability in a robust manner. The models that did not pass the teleconnection criterion usually did so in extreme fashion, by yielding a pattern that was the inverse of that expected. The observed teleconnections are a fundamental statistic that models should endeavor to represent correctly. Even given this uncertainty of the robustness of a single realization, the Brier score and Reproducibility improvements attest to the use of the teleconnection criterion as a useful means for stratifying model performance, and for examining regional interannual variations.

During the Tropical Ocean Global Atmosphere (TOGA) Programme, emphasis was on the ENSO phenomenon, and as such long-lead prediction studies were typically associated with regions that are under its dominant influence. With the advent of the Climate and Variability Predictability Program (CLIVAR), emphasis will also be placed on seasonal to interannual predictability over a wider scope of regions. From the point of view of modelling, we can examine regions that may deserve particular attention with regard to rainfall prediction. To do so, we present in Fig. 21 the Reproducibility for the ECMWF and SNG2 initial condition realizations for each season of the year. Not unexpectedly, the most consistent region of high Reproducibility occurs in the tropics, particularly in the Pacific and Atlantic sectors. Only during summer and winter does the tropical Indian Ocean exhibit coherent Reproducibility in excess of 1. The only regions in which the Reproducibility consistently tends to extend into the subtropics is in the central Pacific and over the maritime continent, and to a lesser degree in the vicinity of the South Pacific

Convergence Zone. Extratropical Reproducibility is confined to northern winter, which is also the time of year when NWP forecasts exhibit their greatest skill, particularly in the Northern Hemisphere where the land/sea temperature contrast dominates the dynamics. Also, this is the time when the Reproducibility is also most extensive in the tropics. This is not to say that these are exclusively the regions for which we may expect to make progress towards increased predictability since the only assumed controlling factor here is the SST. As we come to understand the complex interactions of the various facets of the coupled climate system (atmosphere, hydrosphere, lithosphere, cryosphere) in more depth commensurate gains in predictability should follow.

Acknowledgment. We would like to thank Drs. Julia M. Slingo, Xin-Zhong Liang and David Rowell for insightful comments on an earlier version of this manuscript. We gratefully acknowledge the AMIP modelling groups for making their data available. Prof. Wei-Chyung Wang and Dr. Xin-Zhong Liang kindly provided the initial condition realization simulations of the SUNYA/NCAR Genesis model. We wish to thank Prof. Stefan Hastenrath for providing the observed Nordeste rainfall index, and Drs. David Rowell, Neil Ward and Mike Hulme for providing the observed Sahel rainfall index. This work was performed under the auspices of the U.S. Department of Energy Environmental Sciences Division at the Lawrence Livermore National Laboratory under contract W-7405-ENG-48.

REFERENCES

Aceituno, P., 1988: On the functioning of the Southern Oscillation in the South American sector: Part 1: Surface climate. *Mon. Wea. Rev.*, **116**, 505-524.

Barnett, T. P., 1984: Interaction of the monsoon and Pacific trade wind system at interannual timescales, part3: a partial anatomy of the Southern Oscillation. *Mon. Wea. Rev.*, **112**, 2388-2400.

Barnett, T. P., L. Dümenil, U. Schlese, E. Roeckner and M. Latif, 1989: The effect of Eurasian snow cover on regional and global climate variations. *J. Atmos. Sci.*, **46**, 661-685.

Bhalme, H. N., D. A. Mooley, and S. K. Jadav, 1983: Fluctuations in the drought/flood area over India and relationships with the Southern Oscillation. *Mon. Wea. Rev.*, **111**, 86-94.

Brankovic, C., T. N. Palmer and L. Ferranti, 1994: Predictability of seasonal variations. *J. Clim.*, **7**, 217-237.

Bruce, J. G., J. L. Kerling and W. H. Beatty III, 1985: On the North Brazilian eddy field. *Progress in Oceanography*, Vol. 14, Pergamon, 57-63.

Cadet, D. L., and N. O. Nnoli, 1987: Water vapour transport over Africa and the Atlantic Ocean during summer 1979. *Q. J. R Meteorol. Soc.*, **113**, 581-602.

Chu, P.-S., 1991: Brazil's Climate Anomalies and ENSO. Chap. 3 in *Teleconnections Linking Worldwide Climate Anomalies*. M. Glantz, R. W. Katz and N. Nicholls (eds.), Cambridge University Press. U.K., 535pp.

Covey, D. L., and S. Hastenrath, 1978: The Pacific El Niño and the Atlantic circulation. *Mon. Wea. Rev.*, **106**, 1280-1287.

Critchfield, H. J., 1983: General Climatology, 4th ed., Prentice Hall, Englewood Cliffs, New Jersey.

Dickson, R. R., 1984: Eurasian snow cover versus Indian monsoon rainfall-an extension of Hahn-Shukla results. *J. Clim. Appl. Meteorol.*, **23**, 171-173.

Druyan, L. M., and R. D. Koster, 1989: Sources of Sahel precipitation for simulated drought and rainy seasons. *J. Clim.*, **2**, 1438-1446.

Druyan, L. M., and S. Hastenrath, 1991: Modelling the differential impact of 1984 and 1950 sea-surface temperatures on Sahel rainfall. *Int. J. Clim.*, **11**, 367-380.

Ducoudré, N., K. Laval, and A. Perrier, 1993: SECHIBA, a new set of parametrizations of the hydrologic exchanges at the land atmosphere interface within the LMD atmospheric general circulation model. *J. Clim.*, **6**, 248-273.

Folland, C. K., J. Owen, M. N. Ward and A. Coleman, 1991: Prediction of seasonal rainfall in the Sahel region using empirical and dynamical methods. *J. Forecast.*, **10**, 21-56.

Folland, C. K., T. N. Palmer and D. E. Parker, 1986: Sahel rainfall and worldwide sea temperatures, 1901-1985. *Nature*, **320**, 602-607.

Gates, W. L., 1992: The atmospheric model intercomparison project. *Bull. Amer. Meteorol. Soc.*, **73**, 1962-1970.

Graham, N. E., 1993: Experimental predictions of wet season precipitation in northeastern Brazil. in *Proceedings of the Eighteenth Annual Climate Diagnostics Workshop*, U.S. Department of Commerce, NOAA/NWS/CAC/NMC, Springfield, VA, 378-381.

Hahn, D. J., and J. Shukla, 1976: An apparent relationship between Eurasian snow cover and Indian monsoon rainfall. *J. Atmos. Sci.*, **33**, 2461-2462.

Hameed, S., K. R. Sperber and A. Meinster, 1993: Teleconnections of the Southern Oscillation in the tropical Atlantic sector in the OSU coupled upper ocean-atmosphere GCM. *J. Clim.*, **6**, 487-498.

Hastenrath, S., 1988: Climate and Circulation in the Tropics. 2nd ed., D. Reidel, Boston, Massachusetts. 455pp.

Hastenrath, S., 1990: Prediction of Northeast Brazil rainfall anomalies. *J. Clim.*, **3**, 893-904.

Hastenrath, S., 1994: Extended-range predication in the tropics. in *Proceedings of the International Conference on Monsoon Variability and Prediction*. Vol. II, WMO/TD-No. 619, WCRP-1984, 421-427.

Hastenrath, S., and L. Heller, 1977: Dynamics of climate hazards in Northeast Brazil. *Quart. J. Roy. Meteorol. Soc.*, **103**, 77-92.

Hooky, P., 1970: Revenge of the gods? *Weather*, **25**, 425-428.

Hulme, M., 1994: Validation of large-scale precipitation fields in general circulation models. In *Global Precipitation and Climate Change*, M. Debois and F. Desalmand (eds.), NATO ASI Series, Vol. I 26, Springer-Verlag, Berlin, 387-405.

Jaeger, L., 1983: Monthly and areal patterns of mean global precipitation. in *Variations in the Global Water Budget*. A. Street-Perrott et al. (eds), D. Reidel, Dordrecht, p. 129.

Janowiak, J. E., and P.A. Arkin, 1991: Rainfall variations in the tropics during 1986-89, as estimated from observations of cloud-top temperature. *J. Geophys. Res.*, **96**, 3359-3373.

Joseph, P. V., J. K. Eischeid, and R. J. Pyle, 1994: Interannual variability of the onset of the Indian summer monsoon and its association with atmospheric features, El Niño and sea surface temperature anomalies. *J. Clim.*, **7**, 81-105.

Ju, J., and J. M. Slingo, 1995: The asian summer monsoon and ENSO. *Quart. J. Roy. Meteorol. Soc.*, **121**, 1133-1168.

Lamb, P. J., 1978a: Case studies of tropical Atlantic surface circulation pattern during recent Sub-Saharan weather anomalies: 1967 and 1968. *Mon. Wea. Rev.*, **106**, 482-491.

Lamb, P. J., 1978b: Large-scale tropical Atlantic circulation patterns associated with sub-Saharan Africa weather anomalies. *Tellus*, **30**, 240-251.

Lamb, P. J., and R. A. Peppler, 1991: West Africa. Chap. 5 in *Teleconnections Linking Worldwide Climate Anomalies*. M. Glantz, R. W. Katz and N. Nicholls (eds.), Cambridge University Press. U.K., 535pp.

Lander, J., 1994: The interaction of numerics and physics in a spectral transform GCM. Ph. D. Dissertation, Dept. of Meteorology, Reading University, Reading, England.

Legates, D. R., and C. J. Willmott, 1990: Mean seasonal and spatial variability in gauge-corrected, global precipitation. *Int. J. Clim.*, **10**, 111-127.

Liang, X.-Z., W.-C. Wang, and A. N. Samel, 1996: Predictability of SST anomaly climate signals in two atmospheric general circulation models. *Mon. Wea. Rev.*, (submitted).

Lough, J. M., 1986: Tropical Atlantic sea-surface temperatures and rainfall variations in Subsaharan Africa. *Mon. Wea. Rev.*, **114**, 561-570.

Markham, C. G., and D. R. McLain, 1977: Sea surface temperature related to rain in Ceará, Northeastern Brazil. *Nature*, **265**, 320-323.

Mechoso, C. R., S. W. Lyons and J. A. Spahr, 1990: The impact of sea surface temperature anomalies on the rainfall over Northeast Brazil. *J. Clim.*, **3**, 812-826.

Meehl, G. A., 1994a: Influence of the land surface in the Asian summer monsoon: external conditions versus internal feedbacks. *J. Clim.*, **7**, 1033-1049.

Meehl, G. A., 1994b: Coupled land-ocean-atmosphere processes and South Asian monsoon variability. *Science*, **266**, 263-267.

Molteni, F., R. Buizza, T. N. Palmer, and T. Petroliagis, 1995: The ECMWF ensemble prediction system: Methodology and validation. *Quart. J. Roy. Meteorol. Soc.*, (in press)

Motha, R. P., S. K. Ludec, L. T. Steyaert, C. M. Sakamoto and N. D. Strommen, 1980: Precipitation patterns in West Africa. *Mon. Wea. Rev.*, **109**, 1567-1578.

Moura, A. D., and J. Shukla, 1981: On the dynamics of droughts in Northeast Brazil: Observations, theory and numerical experiments with a general circulation model. *J. Atmos. Sci.*, **38**, 2653-2675.

Murphy, A. H., and R. W. Katz, 1985: Probability, statistics and decision making in the atmospheric sciences. Westview Press, 379-437.

Nicholson, S. E., and D. Entekhabi, 1986: The quasi-periodic behavior of rainfall variability in Africa and its relationship to Southern Oscillation. *Arch. Met. Geoph. Biocl.*, **A34**, 311-348.

Nordeng, T. E., 1996: Extended versions of the convective parametrization scheme at ECMWF and their impact on the mean and transient activity of the model in the tropics. *Q. J. R. Meteorol. Soc.* (submitted).

Palmer, T. N., 1986: Influence of the Atlantic, Pacific and Indian Oceans on Sahel Rainfall. *Nature*, **322**, 251-253.

Palmer, T. N., 1994: Chaos and predictability in forecasting the monsoons. *Proc. Indian Nat. Sci. Acad.*, **60A**, 57-66.

Palmer, T. N., and D. L. T. Anderson, 1994: The prospects for seasonal forecasting-A review paper. *Q. J. R. Meteorol. Soc.*, **120**, 755-793.

Parthasarathy, B., and G. B. Pant, 1984: The spatial nad temporal relationships between the Indian summer monsoon rainfall and the Southern Oscillation. *Tellus*, **36A**, 269-277.

Parthasarathy, B., Kumar, K. R., and Kothawale, D. R., 1992: Indian summer monsoon rainfall indices: 1871-1990. *Meteorol. Mag.*, **121**, 174-186.

Perrone, T. J., and R. G. Miller, 1985: Generalized exponential Markov and model output statistics: a comparative verification. *Mon. Wea. Rev.*, **113**, 1524-1541.

Phillips, T. J., 1994: A summary documentation of the AMIP models. PCMDI Report No. 18, UCRL-ID-116384. Lawrence Livermore National Laboratory, P.O. Box 808, L-264, CA 94551.

Rao, V. B., and V. S. Marques, 1984: Water vapor characteristics over Northeast Brazil during two contrasting years. *J. Clim. App. Meteorol.*, **23**, 440-444.

Rasmusson, E. M., and T. H. Carpenter, 1983: The relationship between eastern equatorial Pacific sea surface temperatures and rainfall over India and Sri Lanka. *Mon. Wea. Rev.*, **111**, 517-528.

Ropelewski, C. F., and Halpert, M. S., 1987: Global and regional scale precipitation patterns associated with the El Niño/Southern Oscillation. *Mon. Wea. Rev.*, **115**, 1606-1626.

Ropelewski, C. F., and Halpert, M. S., 1989: Precipitation patterns associated with the high index phase of the Southern Oscillation. *J. Clim.*, **2**, 268-284.

Rowell, D. P., C. K. Folland, K. Maskell, and M. N. Ward, 1995: Variability of summer rainfall over tropical North Africa (1906-92): Observations and modelling. *Q. J. R. Meteorol. Soc.*, **121**, 669-704.

Schemm, J.-K., S. Schubert, J. Terry, S. Bloom, 1992: Estimates of monthly mean soil moisture for 1979-1989. NASA Tech Memo104571, Goddard Space Flight Center, Greenbelt, MD, 260 pp.

Shukla J., and M. Fennessy, 1994: Simulation and Predictability of Monsoons. in *Proceedings of the International Conference on Monsoon Variability and Prediction.* WMO/TD-No. 619, WCRP-84, Geneva, Switzerland, 567-575.

Slingo, J. M., M. Blackburn, A. Betts, R. Brugge, B. J. Hoskins, M. J. Miller, L. Steenman-Clark, and J. Thuburn, 1994: Mean climate and transience in the tropics of the UGAMP GCM: sensitivity to convective parametrization. *Q. J. R. Meteorol. Soc.*, **120**, 881-922.

Slingo, J. M., K. R. Sperber, J. S. Boyle, J.-P. Ceron, M. Dix, B. Dugas, W. Ebisuzaki, J. Fyfe, D. Gregory, J.-F. Gueremy, J. Hack, A. Harzallah, P. Inness, A. Kitoh, W. K.-M. Lau, B. McAvaney, R. Madden, A. Matthews, T. N. Palmer, C.-K. Park, D. Randall, N. Renno, 1996: Intraseasonal oscillations in 15 atmospheric general circulation models: Results from an AMIP diagnostic subproject. *Clim. Dynam.*, (in press).

Spencer, R. W., 1993: Global oceanic precipitation from the MSU during 1979-91 and comparison to other climatologies. *J. Clim.*, **6**, 1301-1326.

Sperber, K. R., and S. Hameed, 1993: Phase locking of Nordeste precipitation with sea surface temperatures. *Geophys. Res. Lett.*, **20**, 113-116.

Sperber, K. R., and T. N. Palmer, 1994: Atmospheric model intercomparison project: Monsoon simulations. Proc. of the International Conference on Monsoon Variability and Prediction. 9-13 May 1994, Trieste, Italy.

Tanaka, M., B. C. Weare, A. R. Navajo, R. E. Newell, 1975: Recent African rainfall patterns. *Nature*, **255**, 201-203.

Ward, M. N., and C. K. Folland, 1991: Prediction of seasonal rainfall in the north Nordeste of Brazil using eigenvectors of sea-surface temperature. *Int. J. Climatol.*, 11, 711-743.

Ward, M. N., S. Brooks and C. K. Folland, 1988: of seasonal rainfall in the northern Nordeste region of Brazil. Chap. 21 in Recent Climatic Change: A regional approach. S. Gregory (ed.), Belhaven Press, NY, 237-251.

Webster, P. J. and Yang, S., 1992: Monsoon and ENSO: selectively interactive systems. *Quart. J. Roy. Meteorol. Soc.*, **118**, 877-926.

WMO, 1992: Simulation of interannual and intraseasonal monsoon variability. WMO/TD-No. 470, 185pp.

WMO, 1993: Simulation and prediction of monsoons: Recent results. WMO/TD-No. 546, Geneva, Switzerland, 73pp.

Woodruff, S. D., R. J. Slutz, R. L. Jenne and P. M. Steurer, 1987: A comprehensive ocean-atmosphere data set. *Bull. Amer. Meteorol. Soc.*, **68**, 1239-1250.

Fig. 1. Observed and simulated June/July/August/September(JJAS) averaged precip
itation and 850hPa wind climatologies in the vicinity of the Asian summer monsoon
The observed rainfall climatology is based on the MSU/raingauge data set for the pe
riod 1979-88. The JJAS station rainfall data was not available for the full 10 years a
some land points, primarily in the vicinity of China, and several grid points north an
east of the Bay of Bengal, and data was considered to be missing if less than 6 year
were available from which to construct the time mean field (shaded black). Precipita
tion contours are plotted at 2, 5, 10 and 20 mm day^{-1}. The 850hPa flow is based o
ECMWF analyses for 1980-89. The isotachs are plotted at an interval of 5m s^{-1}.

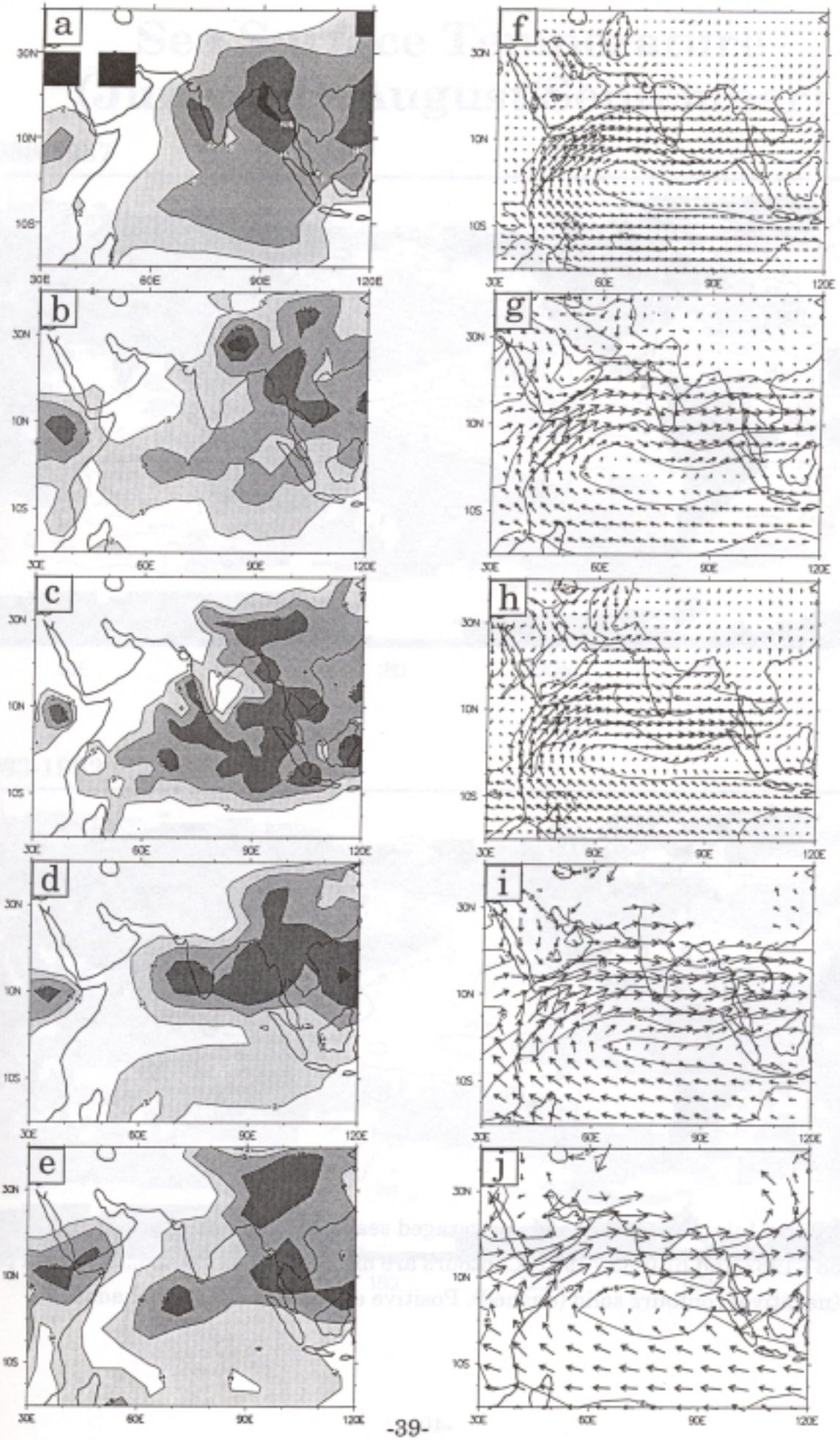
a
b
c
d
e
f
g
h
i
j
30N
10N
10S
30E
60E
90E
120E

Fig. 2. June/July/August/September averaged sea surface temperature anomalies fo
a) 1988 - 1987 and b) 1983 - 1982. Contours are drawn at 0.5, 1.0, 1.5,... °C with po
itive (negative) contours solid (dashed). Positive anomalies are grey-shaded.

Sea Surface Temperature (June/July/August/September)

1988-1987

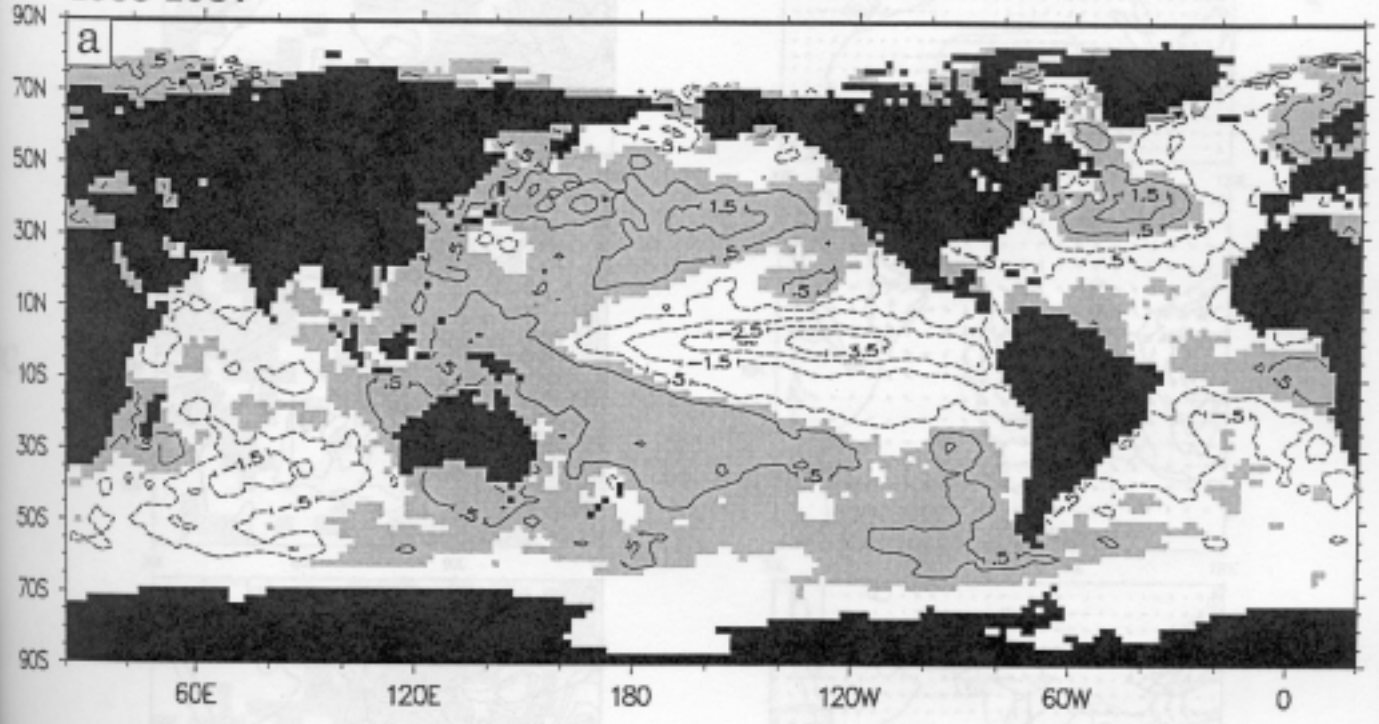

1983-1982

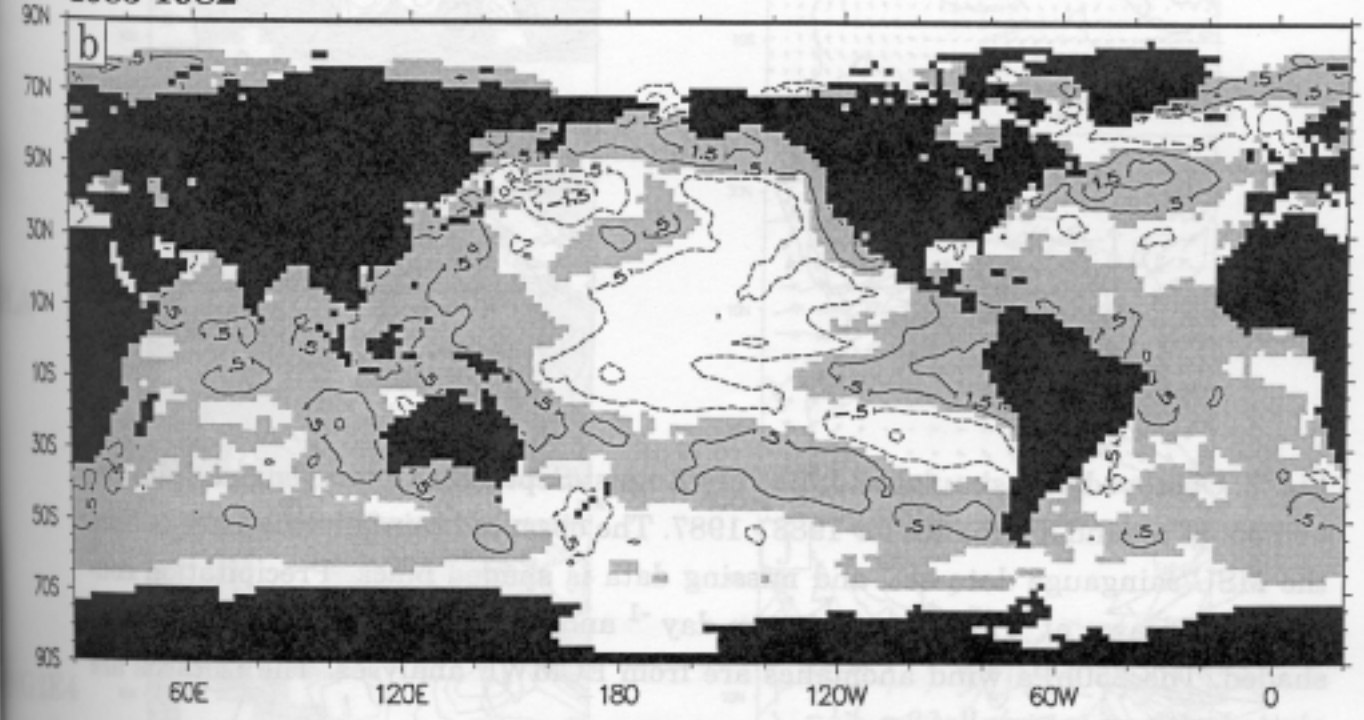

Fig. 3. Observed and simulated June/July/August/September averaged precipitation and 850hPa wind anomalies for 1988 - 1987. The observed rainfall difference is from the MSU/raingauge data set, and missing data is shaded black. Precipitation contours are drawn at 1, 2, 4, 8, 12,... mm day $^{-1}$ and the positive anomalies are grey shaded. The 850hPa wind anomalies are from ECMWF analyses. The isotachs are plotted with an interval of 2m s^{-1}.

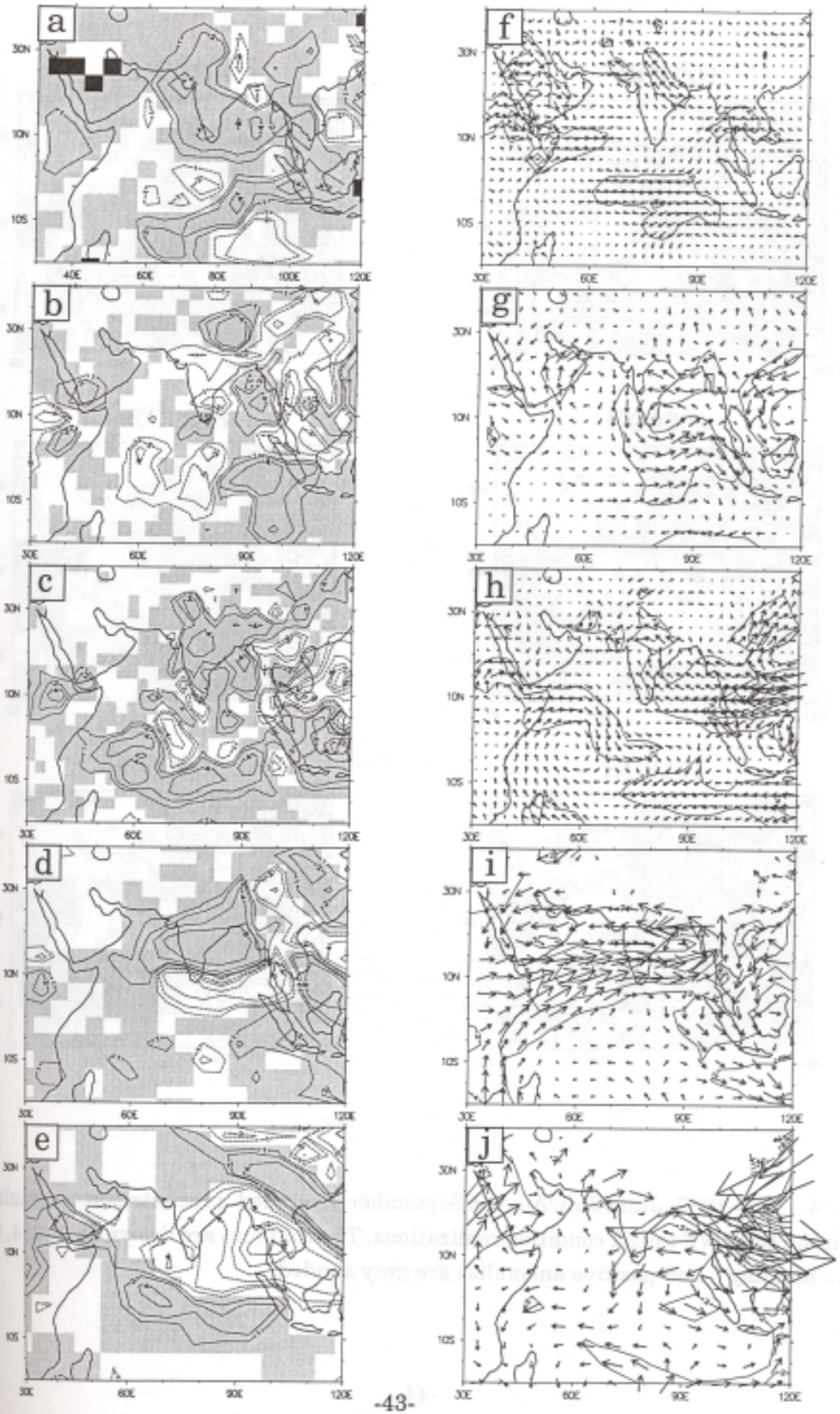
Rainfall
850hPa wind
a
b
c
d
e
f
g
h
i
j
30N
10N
10S
40E
60E
80E
100E
120E
30E
90E

Fig. 4. 1988-1987 June/July/August/September averaged precipitation anomalies from the ECMWF initial condition realizations. The contours are drawn at 1, 2, 4, 8, 12,... mm day^{-1} and positive anomalies are grey-shaded.

EC9104

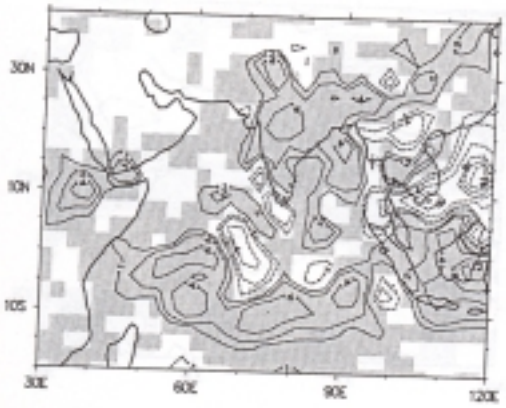

EC9201

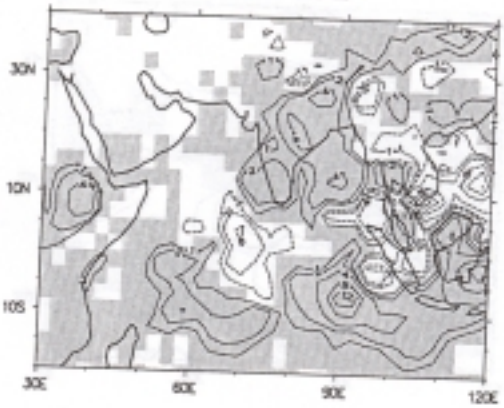

EC9203

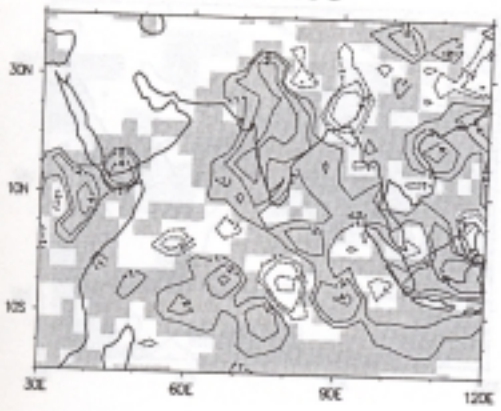

EC9204

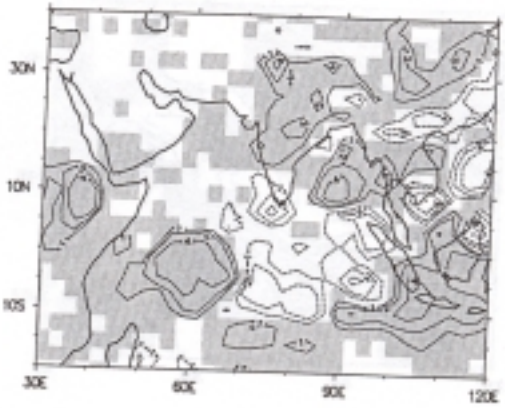

EC9301

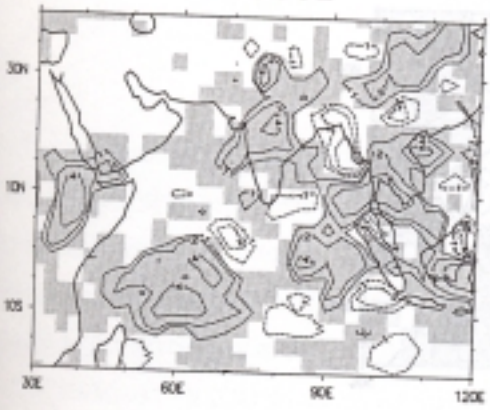

EC9401

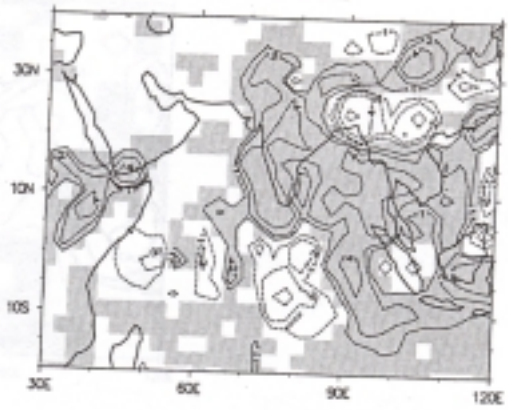

Fig. 5. As Fig. 4 but for the SUNY/NCAR Genesis 2 initial condition realizations.

SNG2E1

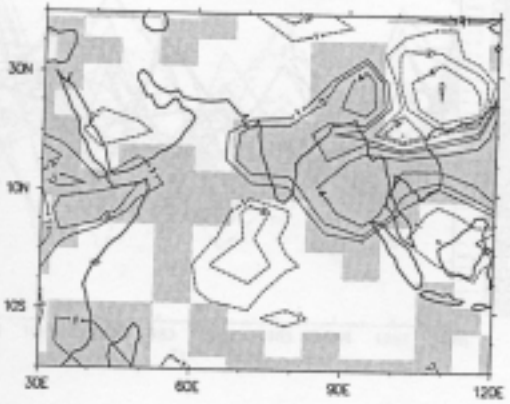

SNG2E2

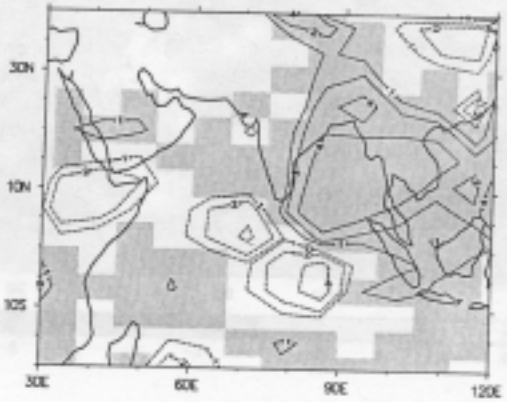

SNG2E3

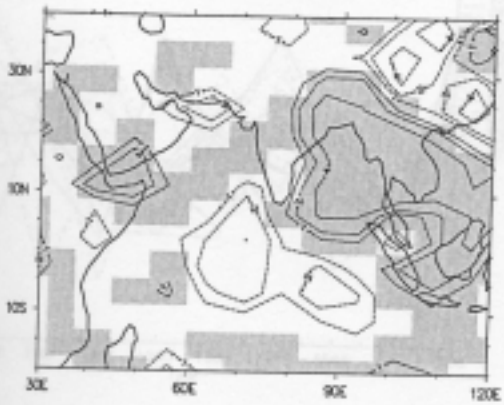

SNG2E4

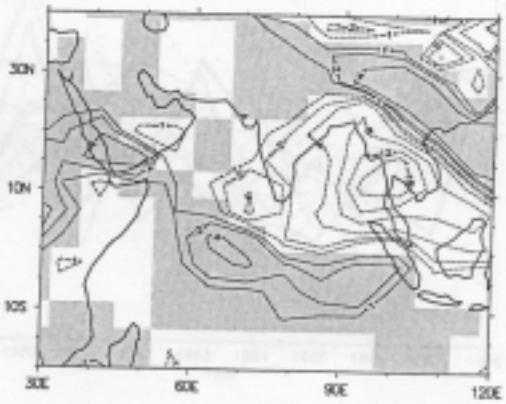

SNG2E5

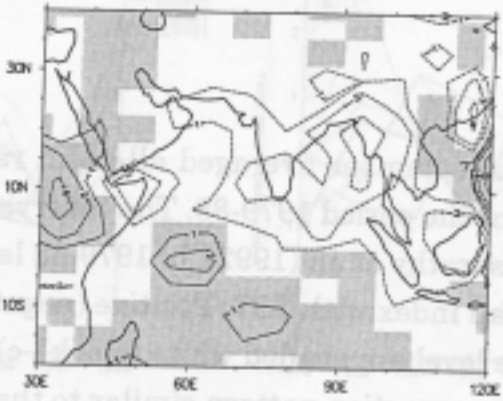

Fig. 6. a) June/July/August/September averaged all-India rainfall indices from the suite of AMIP simulations for the period 1979-88. The observations (heavy black solid line) are taken from Parthasarathy et al. (1992), b) 1979-88 lag zero teleconnection of the observed all-India rainfall index with SST. Positive (negative) correlations significant at the 95% confidence level are shaded white (black). c) rainfall indices of those models that simulated a teleconnection pattern similar to that in (b), d) rainfall indices of those models that did not simulate a teleconnection pattern similar to that in (b), e) rainfall indices of the ECMWF initial condition realizations, f) rainfall indices of the SUNY/NCAR Genesis 2 initial condition realizations. The indices are land only (based on each models land/sea mask to isolate India) and area-weighted. For each model and the observations the index has been normalized by removal of their respective mean and division by their standard deviation.

Indian Rainfall Index (JJAS)

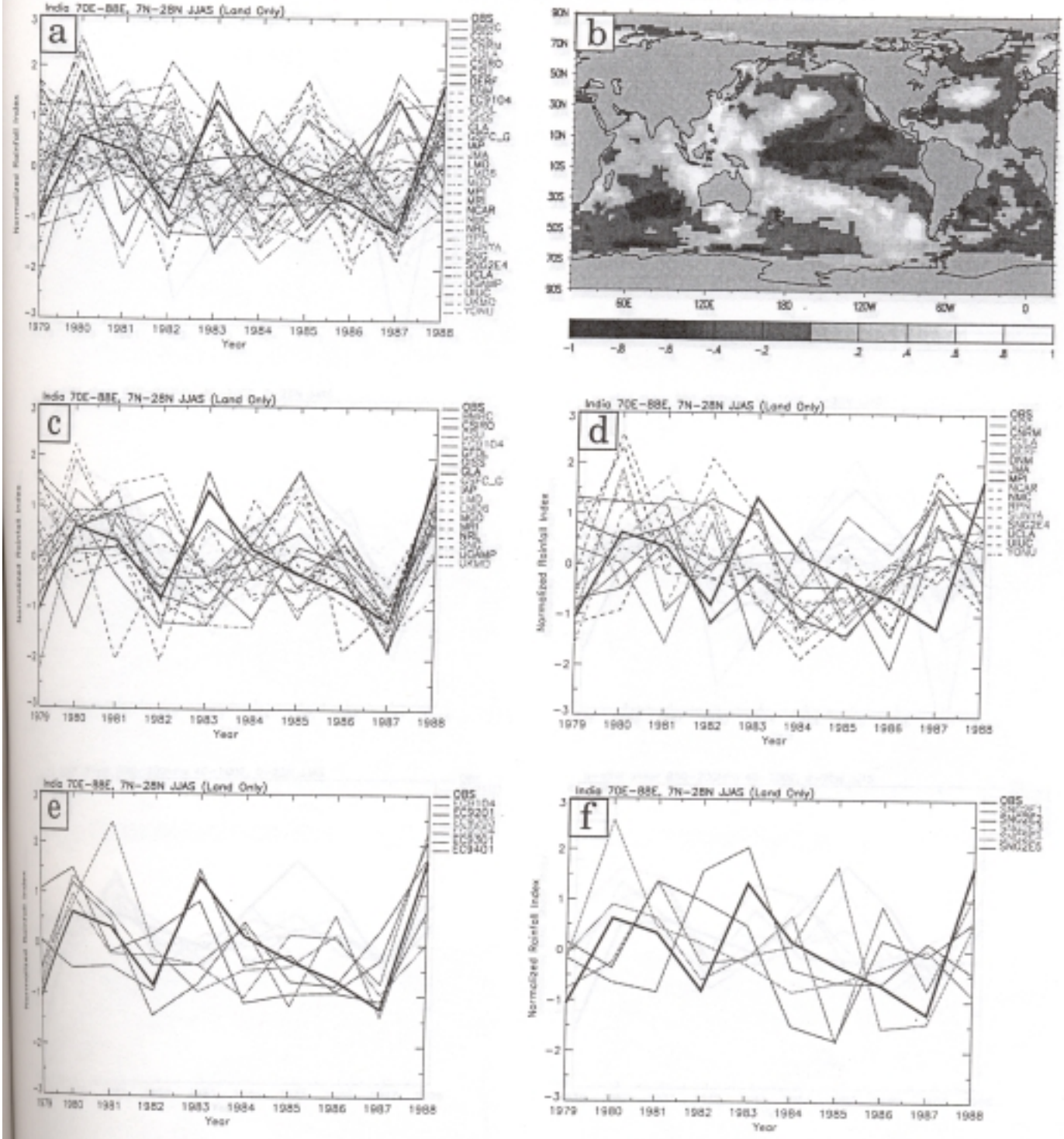

Fig. 7. As Fig. 6 but for the 850-200hPa normalized zonal wind shear indices based on the region 40-100°E, 0-25°N. Note: the reduced set of dynamical indices presented in (c) is for the same models shown in Fig. 6c.

Monsoon Windshear Index (JJAS)

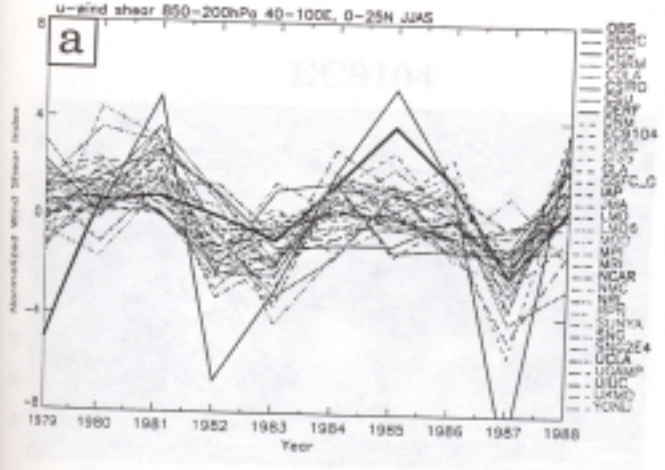

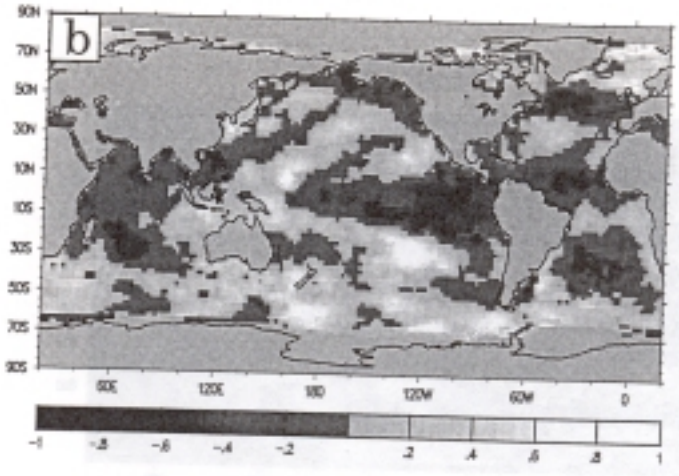

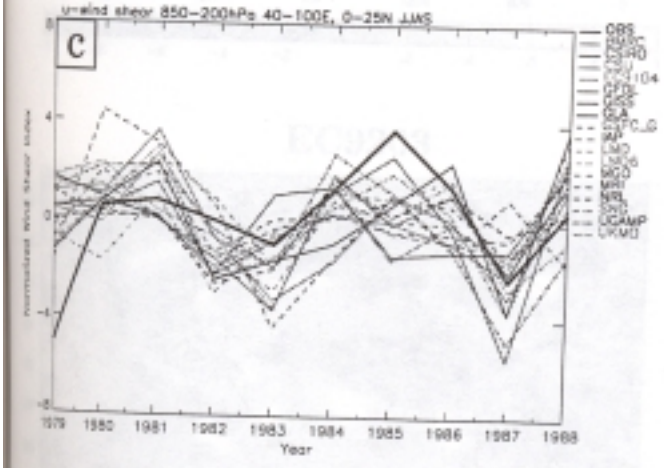

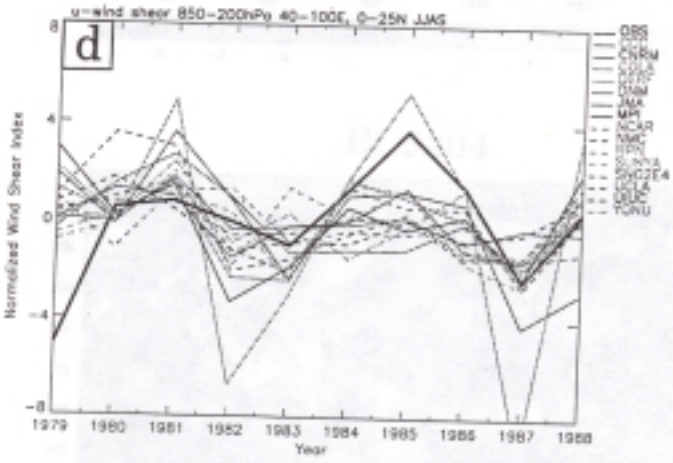

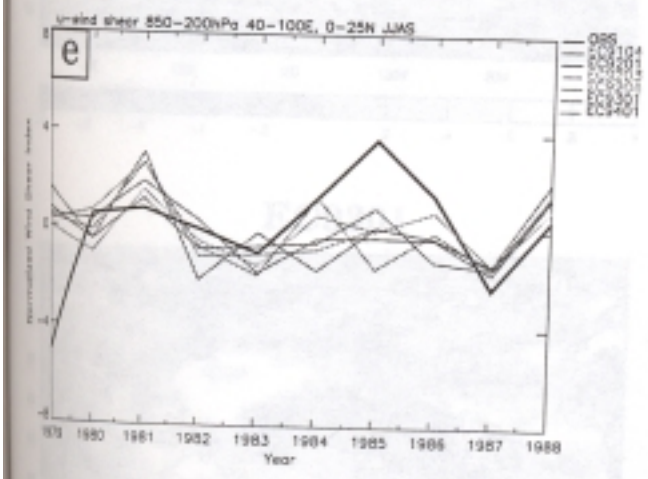

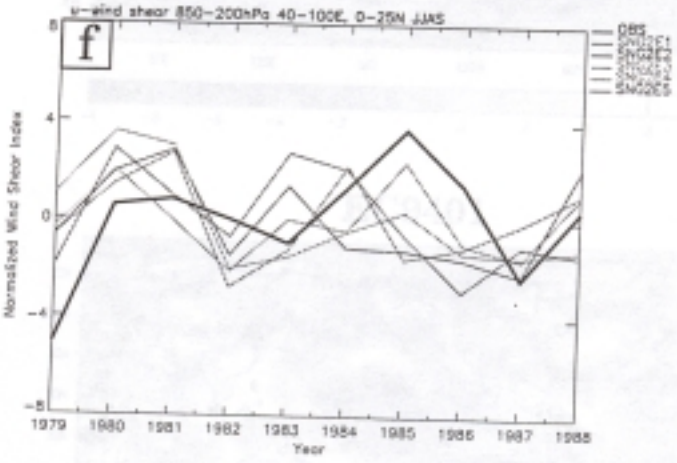

Fig. 8. 1979-88 lag zero teleconnections of the June/July/August/September averaged all-India rainfall indices with SST from the ECMWF initial condition realizations.

EC9104

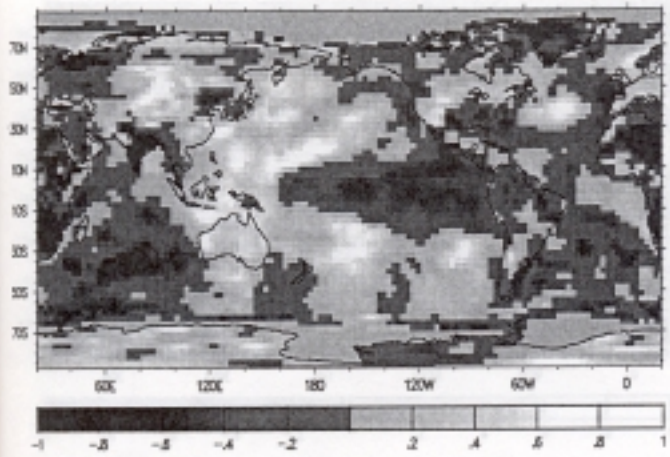

EC9201

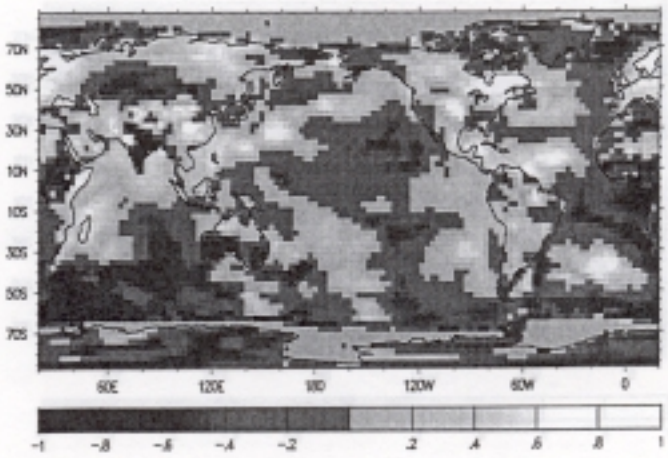

EC9203

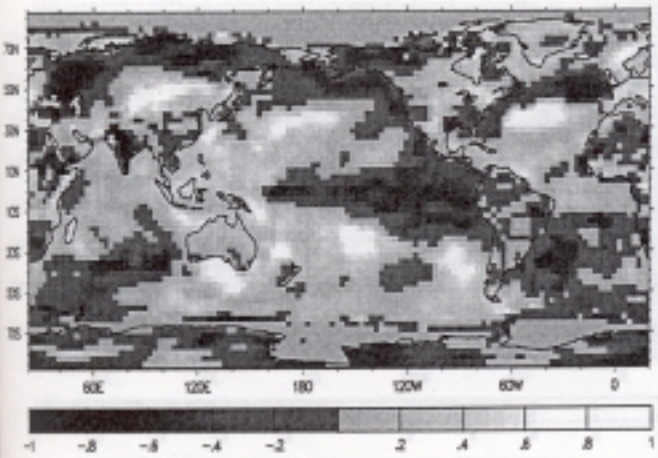

EC9204

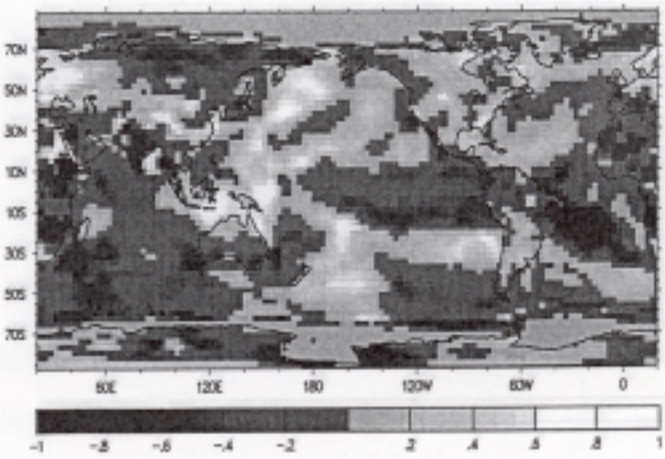

EC9301

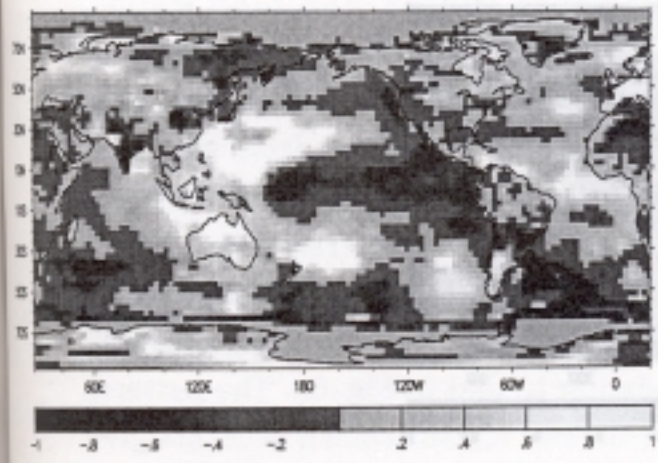

EC9401

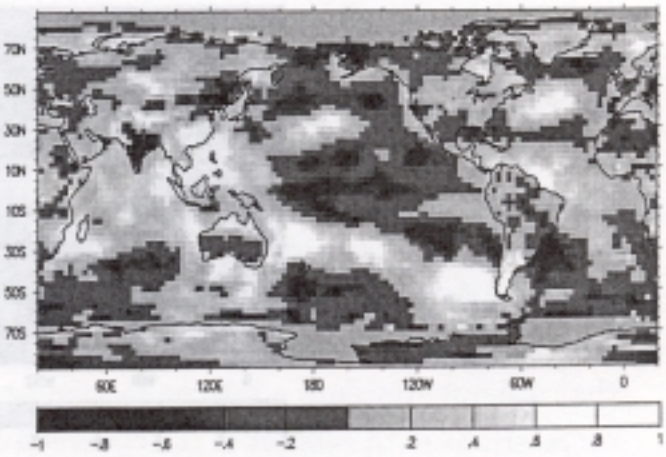

Fig. 9. As Fig. 8 but for the SUNY/NCAR Genesis 2 initial condition realizations.

SNG2E1

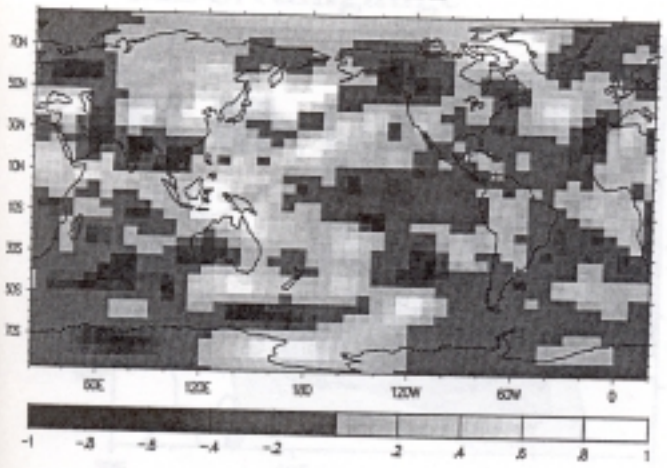

SNG2E2

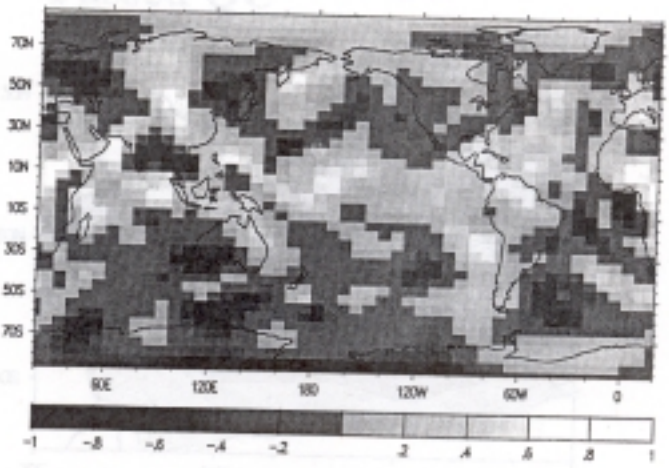

SNG2E3

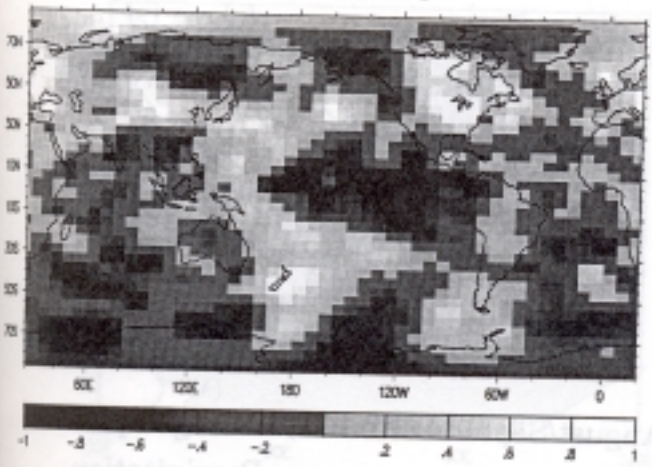

SNG2E4

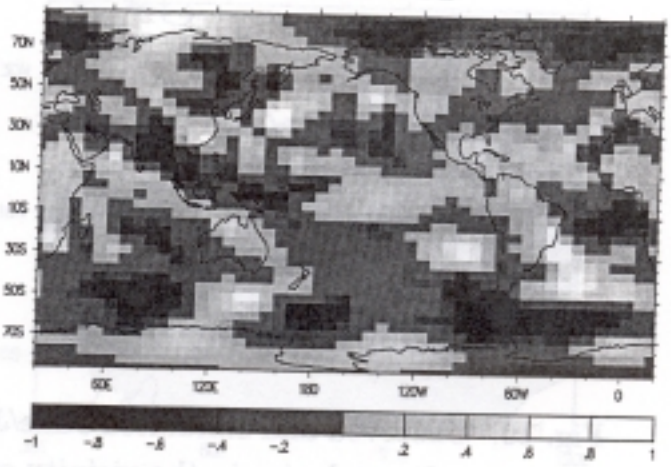

SNG2E5

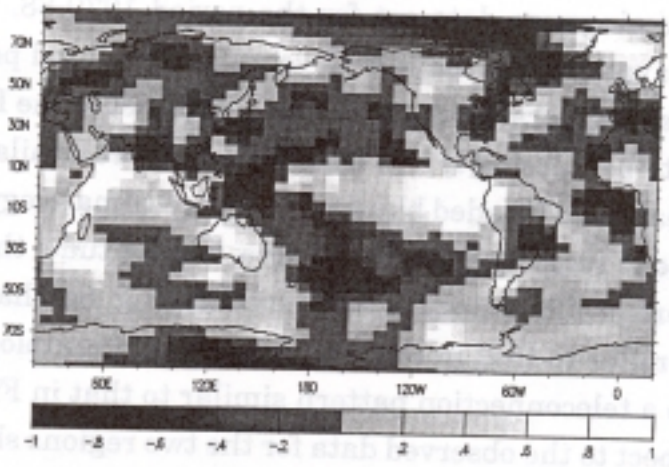

Fig. 10. Observed and simulated June/July/August/September(JJAS) averaged precipitation climatologies in the vicinity of the Asian summer monsoon. Precipitation contours are plotted at 2, 4, 8, and 16 mm day^{-1}. a) The observed rainfall climatology is based on the MSU/raingauge data set for the period 1979-88. The JJAS station rainfall data was not available for the full 10 years at some land points, primarily in the vicinity of China, and several grid points north and east of the Bay of Bengal, and data was considered to be missing if less than 6 years were available from which to construct the time mean field (shaded black). b) average climatology of all AMIP models (all models have been regridded to 4^0 latitude x 5^0 longitude, the resolution of the observed data). c) average climatology of those models (Fig. 6c) that simulated a teleconnection pattern similar to that in Fig. 6b. d) average climatology of those models that did not simulate a teleconnection pattern similar to that in Fig. 6b. The pattern correlations with respect to the observed data for the two regions shown in (a) are given in the top right of each model panel. The upper (lower) value is associated with the larger (smaller) region.

JJAS Rainfall Climatologies

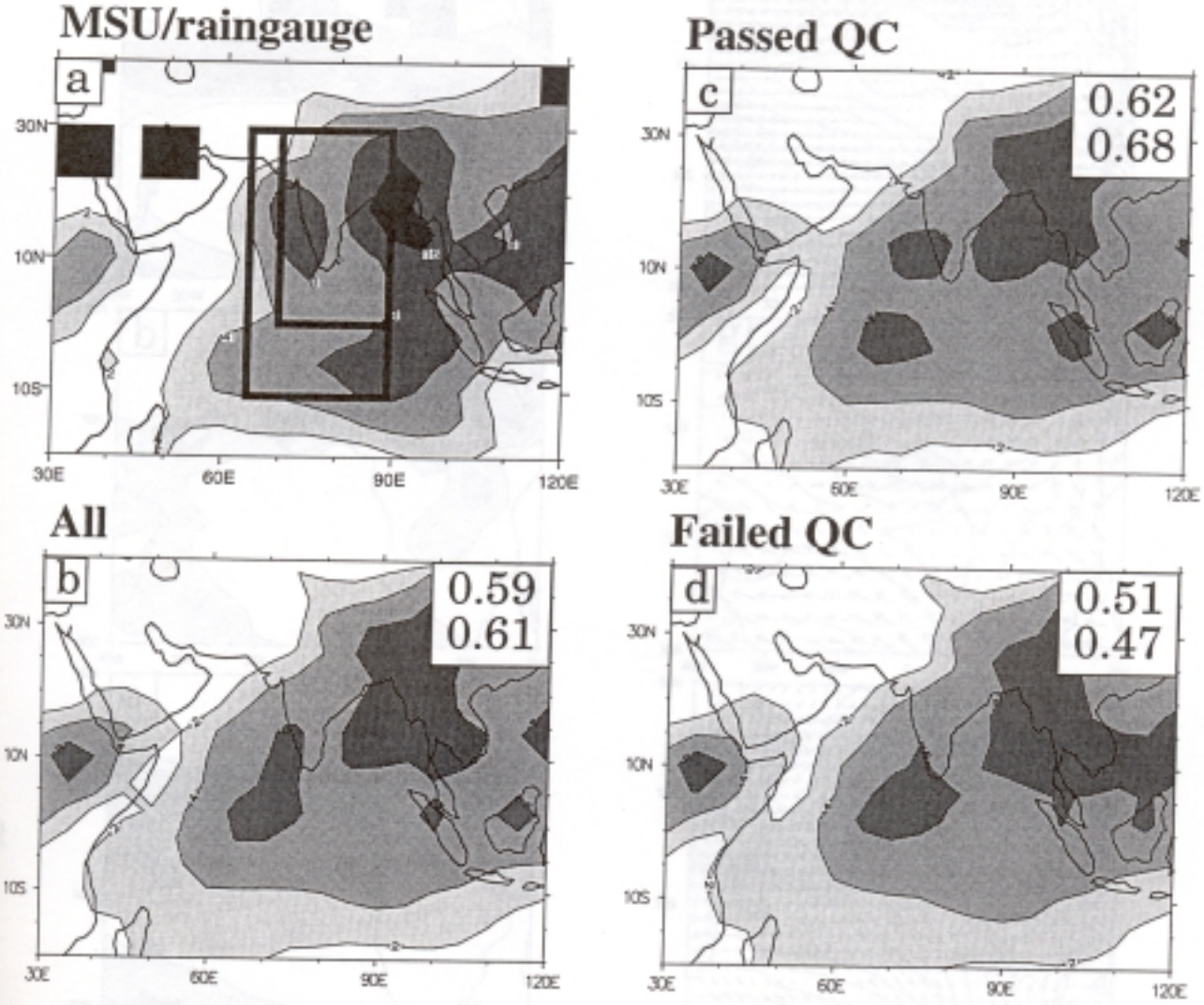

Fig. 11 Observed and simulated July/August/September (JAS) averaged precipitation and 850hPa wind climatologies in the vicinity of Africa. The JAS station rainfall data was not available for the full 10 years at many land points over Africa (10^0-25^0E, 22^0S-30^0N, and the western Sahara Desert), and data was considered to be missing if less than 7 years were available from which to construct the time mean field (shaded black). Precipitation contours are plotted at 2, 5, 10 and 20mm day^{-1}. The 850hPa flow is based on ECMWF analyses for 1980-89. Isotachs are plotted at with an interval of 2m s^{-1}.

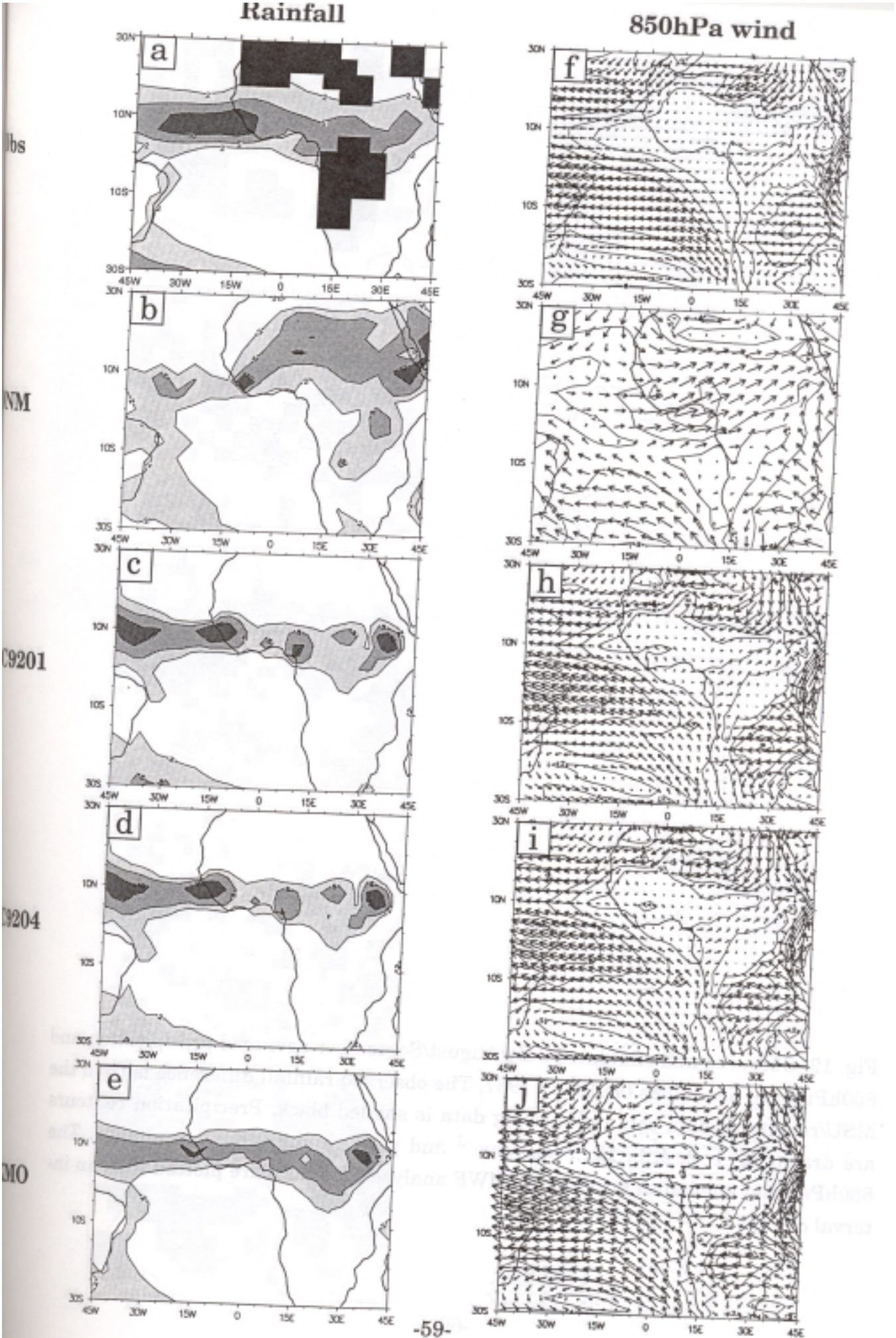

Obs

NM

C9201

C9204

MO

Fig. 12. Observed and simulated July/August/September averaged precipitation and 850hPa wind anomalies for 1988 - 1987. The observed rainfall difference is from the MSU/raingauge data set, and missing data is shaded black. Precipitation contours are drawn at 1, 2, 4, 8, 12,... mm day $^{-1}$ and positive anomalies are shaded. The 850hPa wind anomalies are from ECMWF analyses. Isotachs are plotted with an interval of 1m s^{-1}.

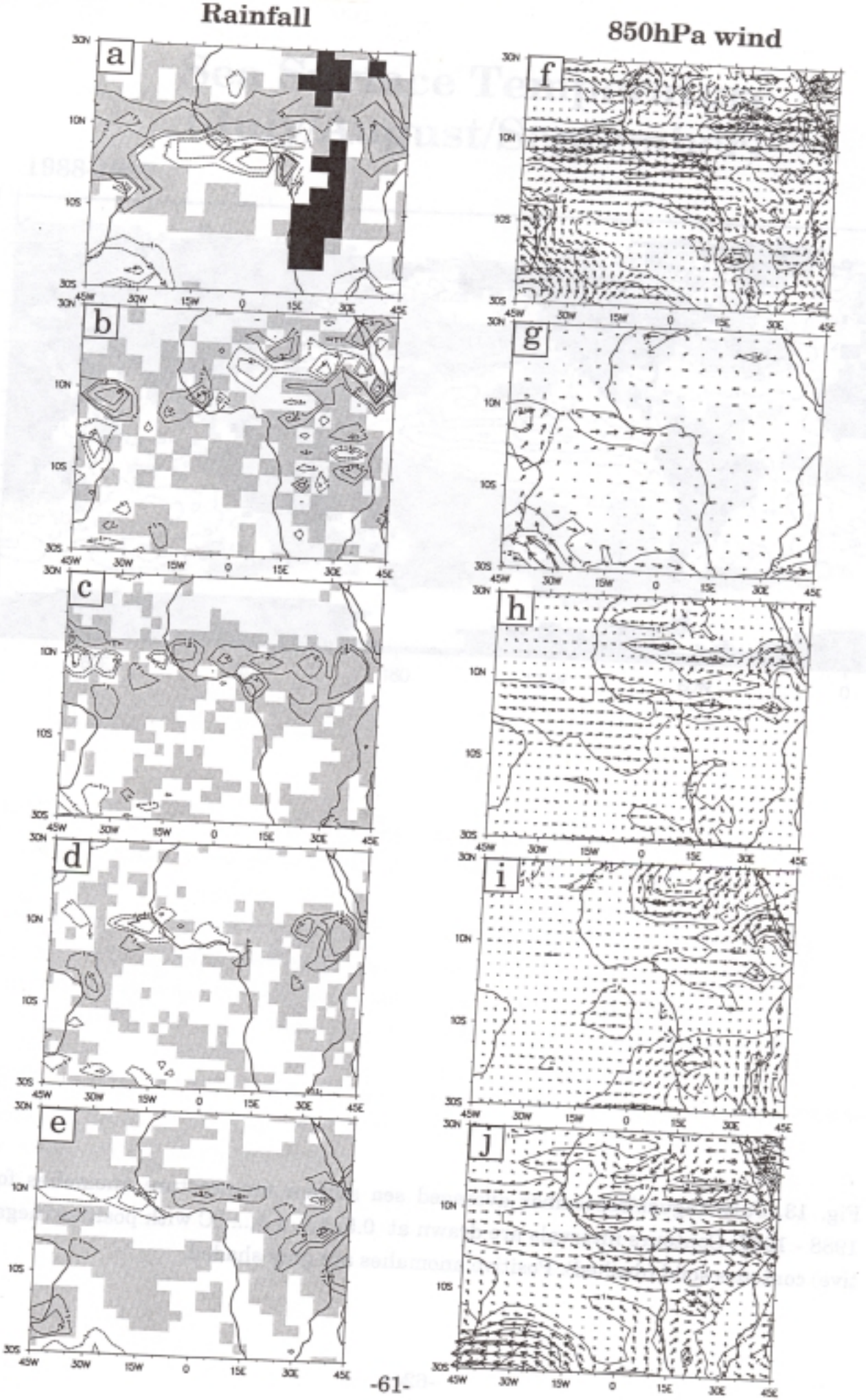
Rainfall
850hPa wind
a
b
c
d
e
f
g
h
i
J
30N
10N
10S
30S
45W
30W
15W
0
15E
30E
45E

-61-

Fig. 13. July/August/September averaged sea surface temperature anomalies for 1988 - 1987. Contours intervals are drawn at 0.5, 1.0, 1.5,... ^{o}C with positive (negative) contours solid (dashed). Positive anomalies are grey-shaded.

Sea Surface Temperature (July/August/September)

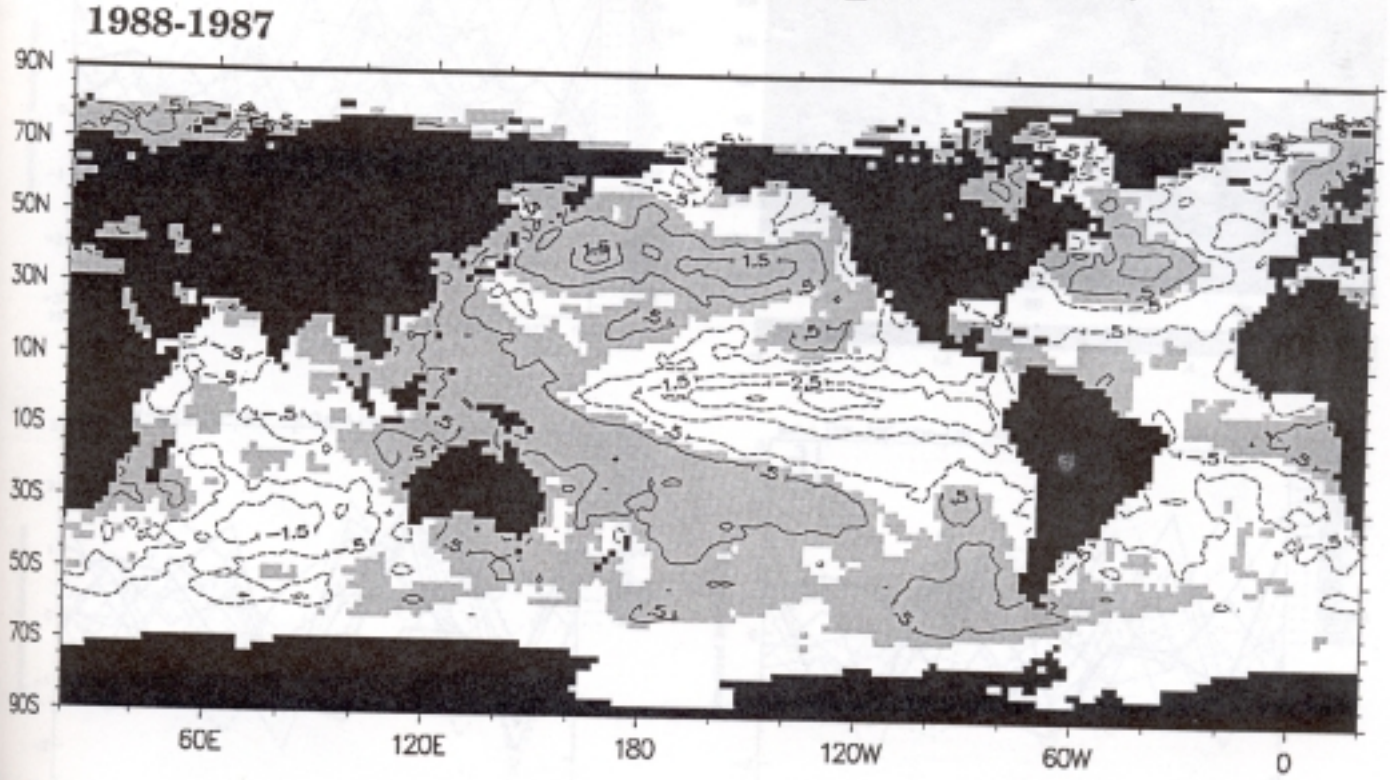

Fig. 14. a) July/August/September averaged Sahel rainfall indices from the suite of AMIP simulations for the period 1979-88. The observations (heavy black solid line) were provided by Rowell and Ward (1991, personal communication) and are based on the station data of Sharon Nicholson through 1984, with subsequent updates provided by the Hadley Centre, b) 1979-88 lag zero teleconnection of the observed Sahel rainfall index with SST, c) rainfall indices of those models that simulated a teleconnection pattern similar to that in (b), d) rainfall indices of those models that did not simulate a teleconnection pattern similar to that in (b), e) rainfall indices of the ECMWF initial condition realizations, f) rainfall indices of the SUNY/NCAR Genesis 2 initial condition realizations. The indices are land only (15°W-38°E, 12-18°N, based on each models land/sea mask) and area-weighted. For each model and the observations the index has been normalized by removal of their respective mean and division by their standard deviation. In (b) positive (negative) correlations significant at 95% confidence level are shaded white (black).

Sahel Rainfall Index (JAS)

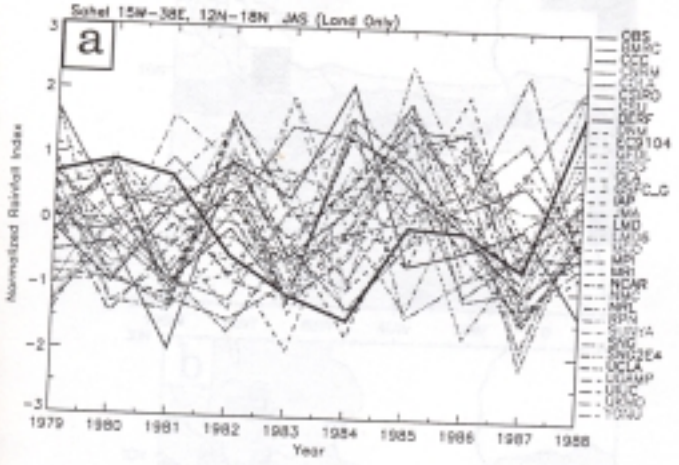

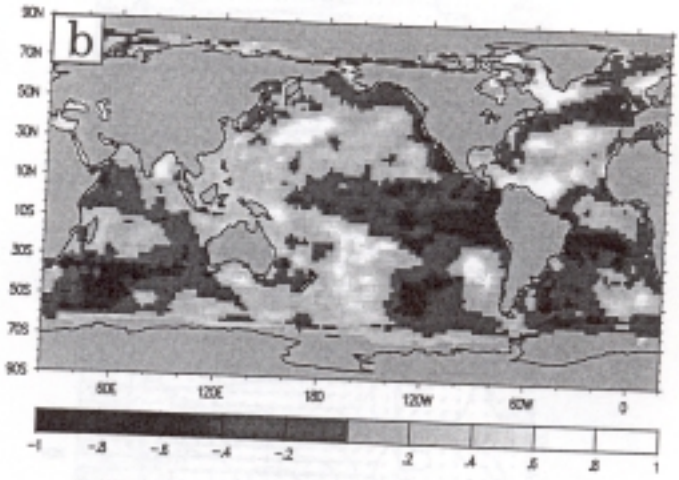

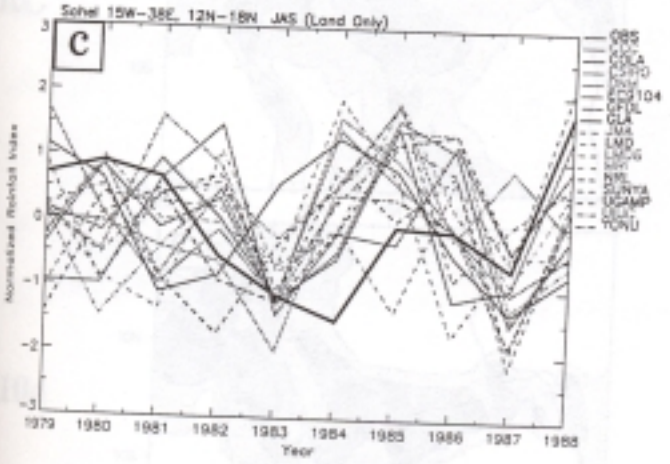

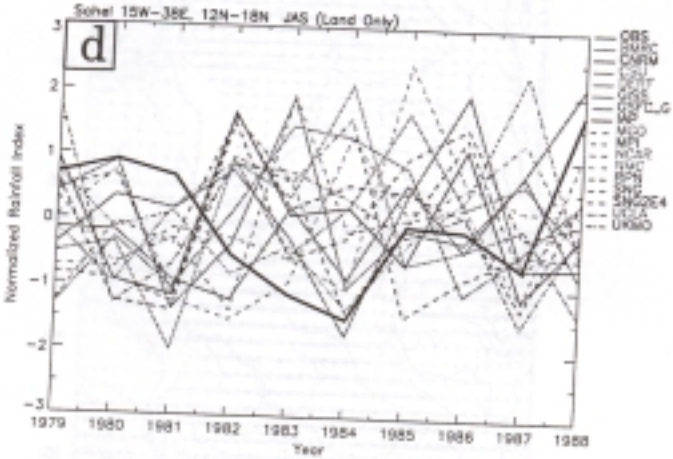

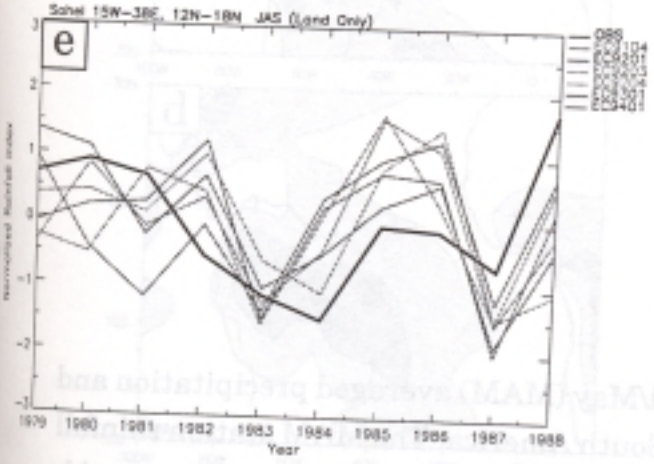

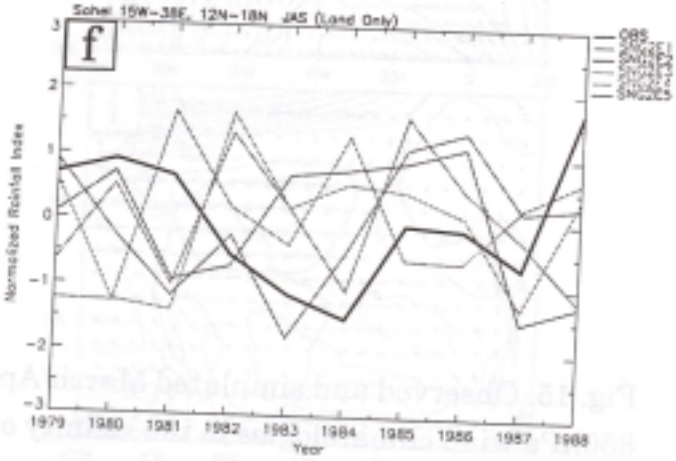

Fig. 15. Observed and simulated March/April/May (MAM) averaged precipitation and 850hPa wind climatologies in the vicinity of South America. The MAM station rainfall data was not available for the full 10 years at some land points, and data was considered to be missing if less than 7 years were available from which to construct the time mean field (shaded black). Precipitation contours are plotted at 2, 5, 10 and 20 mm day^{-1}. The 850hPa flow is based on ECMWF analyses for 1980-89. Isotachs are plotted with an interval of 2m s^{-1}.

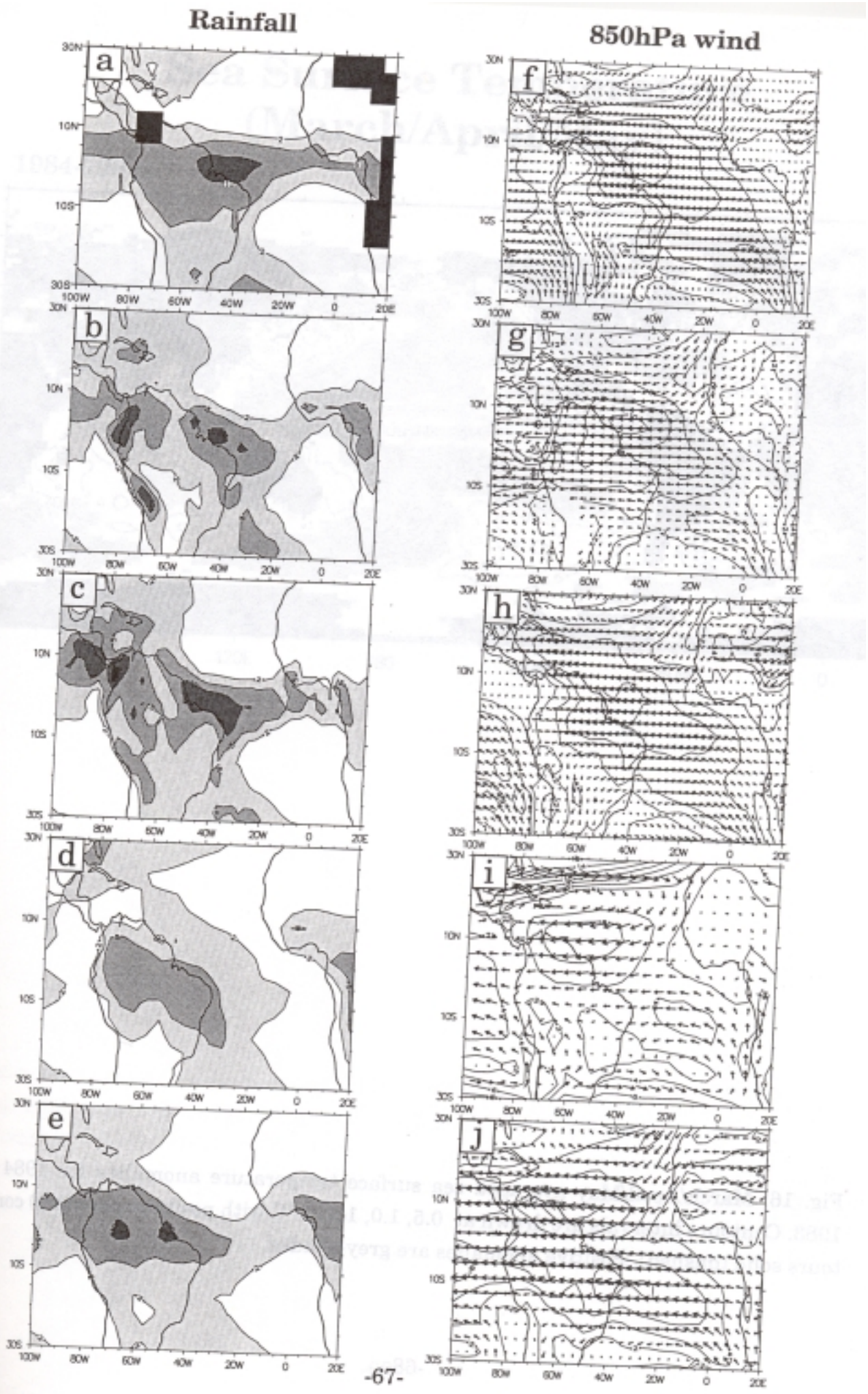
Rainfall
850hPa wind
a
b
c
d
e
f
g
h
i
J
30N
10N
10S
30S
100W
80W
60W
40W
20W
0
20E

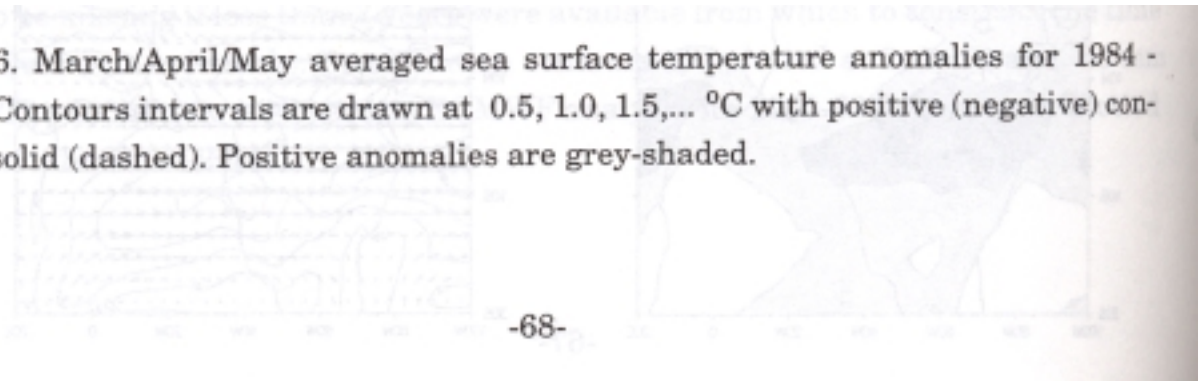

Fig. 16. March/April/May averaged sea surface temperature anomalies for 1984 - 1983. Contours intervals are drawn at 0.5, 1.0, 1.5,... ^{o}C with positive (negative) contours solid (dashed). Positive anomalies are grey-shaded.

Sea Surface Temperature (March/April/May)

1984-1983

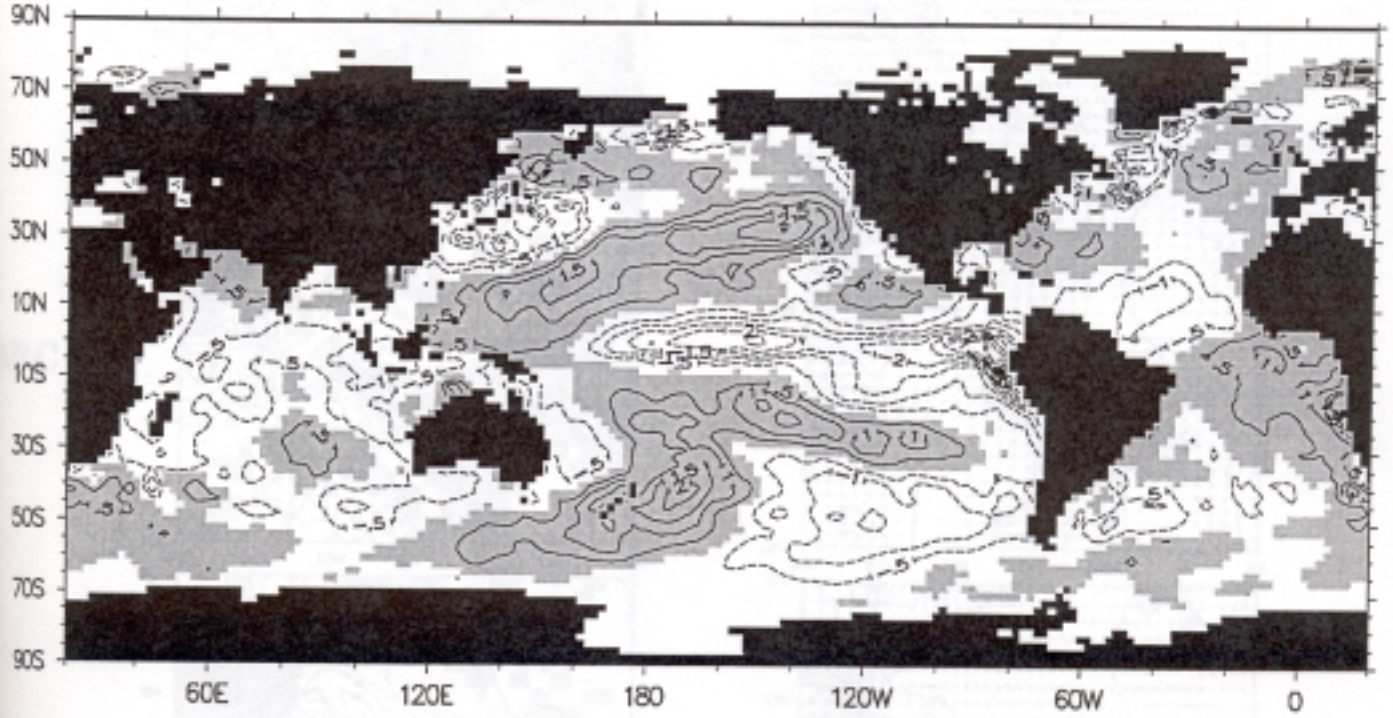

Fig. 17. Observed and simulated March/April/May averaged precipitation and 850hPa wind anomalies for 1984 - 1983. The observed rainfall difference is from the MSU/raingauge data set, and missing data is shaded black. Precipitation contours are drawn at 1, 2, 4, 8, 12,... mm day $^{-1}$ and positive anomalies are grey-shaded. The 850hPa wind anomalies are from ECMWF analyses. Isotachs are plotted with an interval of 2m s^{-1}.

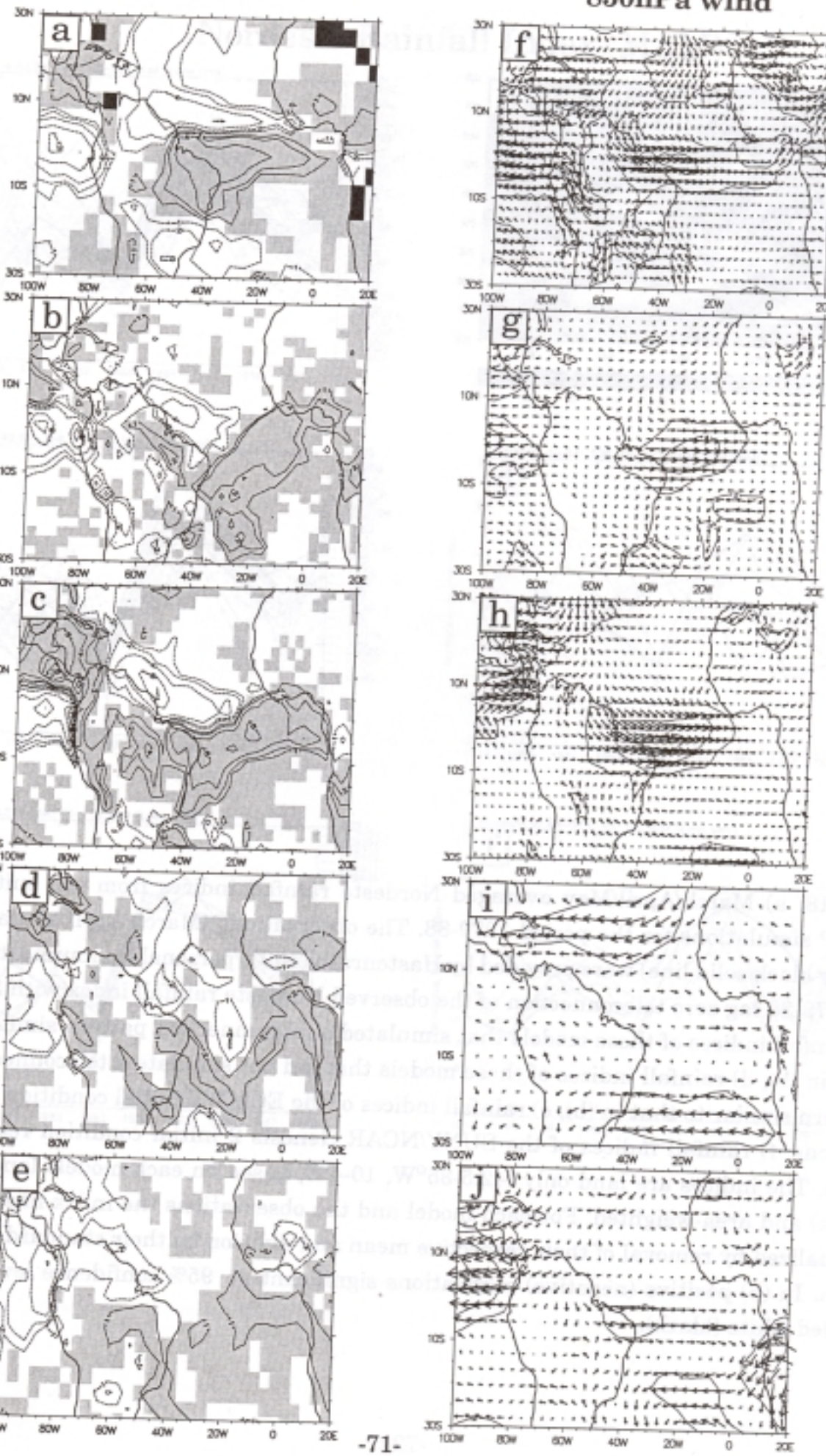
Rainfall
850hPa wind
a
b
c
d
e
f
g
h
i
J
30N
10N
10S
30S
100W
80W
60W
40W
20W
0
20E

Fig. 18. a) March/April/May averaged Nordeste rainfall indices from the suite of AMIP simulations for the period 1979-88. The observations (March/April averaged, heavy black solid line) were provided by Hastenrath (1991, personal communication), b) 1979-88 lag zero teleconnection of the observed Nordeste rainfall index with SST, c) rainfall indices of those models that simulated a teleconnection pattern similar to that in (b), d) rainfall indices of those models that did not simulate a teleconnection pattern similar to that in (b), e) rainfall indices of the ECMWF initial condition realizations, f) rainfall indices of the SUNY/NCAR Genesis 2 initial condition realizations. The indices are land only (42.5-35°W, 10-4°S, based on each models land/sea mask) and area-weighted. For each model and the observations the index has been normalized by removal of their respective mean and division by their standard deviation. In (b) positive (negative) correlations significant at 95% confidence level are shaded white (black).

Nordeste Rainfall Index (MAM)

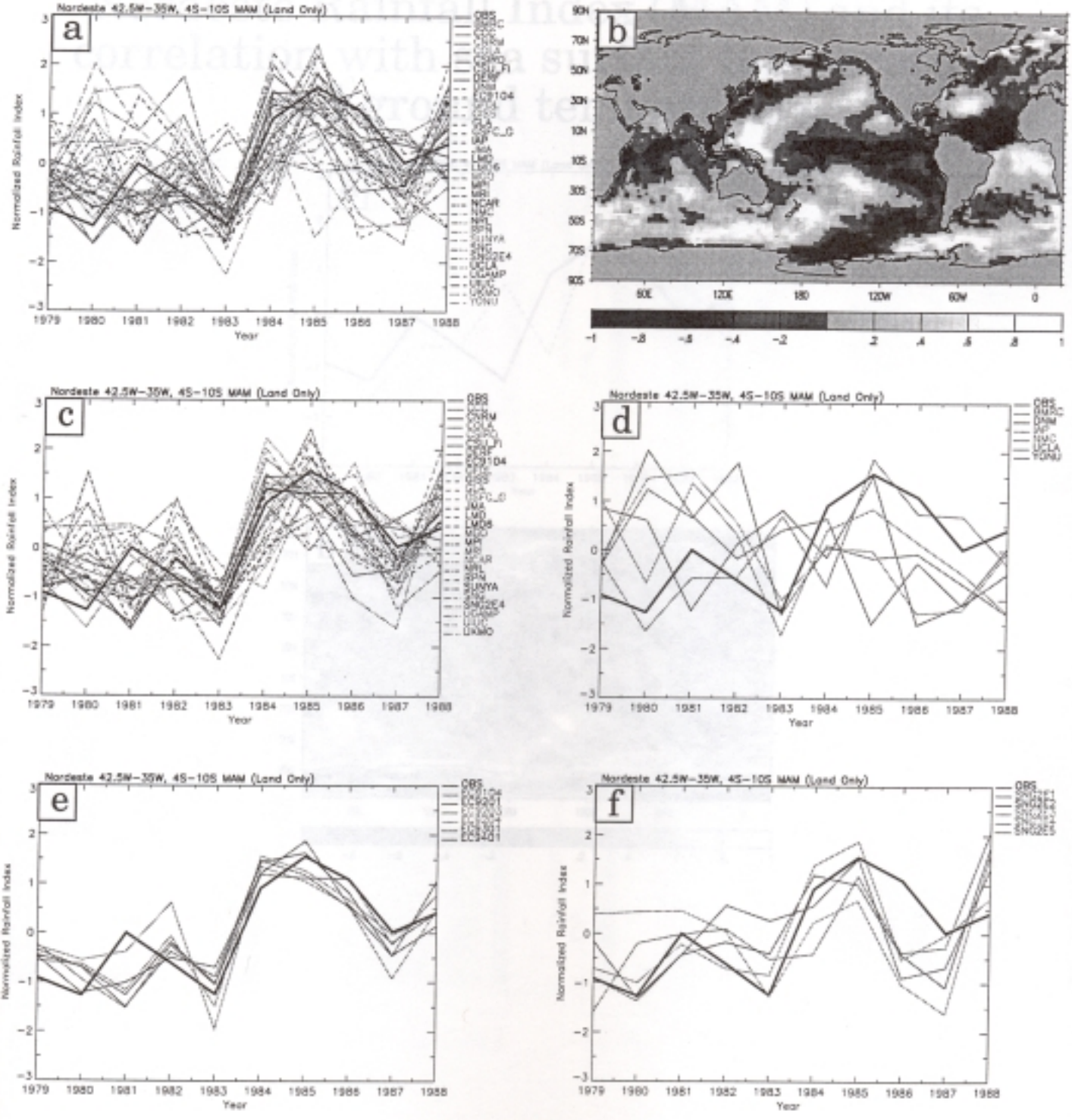

Fig. 19. a) as Fig. 18a but for the BMRC model, b) as Fig. 18b but for the BMRC model.

BMRC
Nordeste Rainfall Index (MAM) and its correlation with sea surface temperature and ground temperature

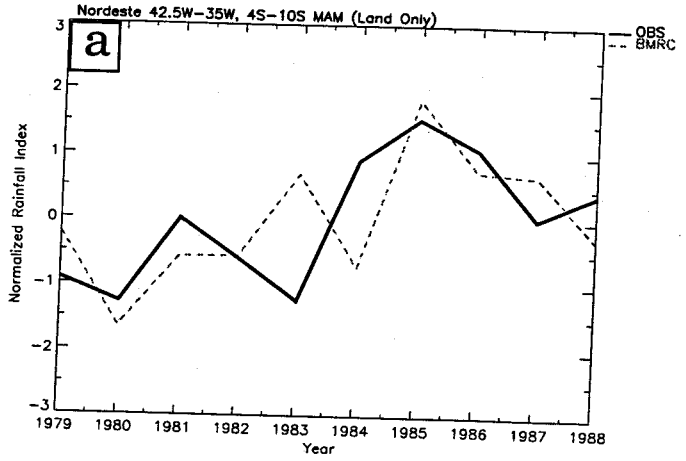

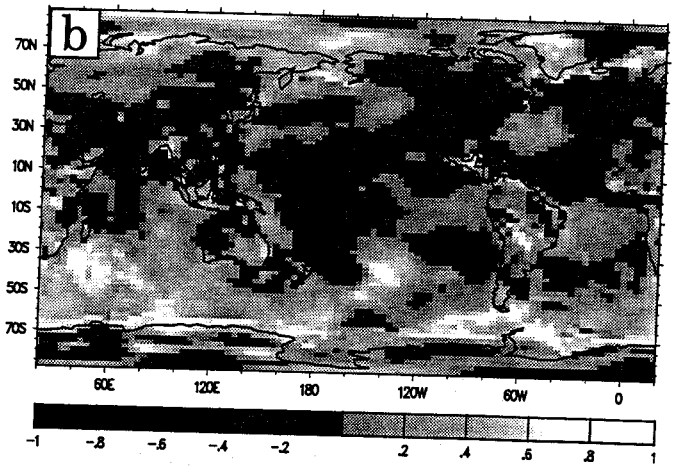

Fig. 20. All-India and Sahel rainfall/SST teleconnection sensitivity to horizontal resolution, convective parametrization closure, and numerics. The models are ordered from low to high horizontal resolution. Moisture (light-shaded) versus buoyancy closure (dark shaded) a) India b) Sahel. Gridpoint (light shaded) versus spectral (dark-shaded) numerics c) India d) Sahel.

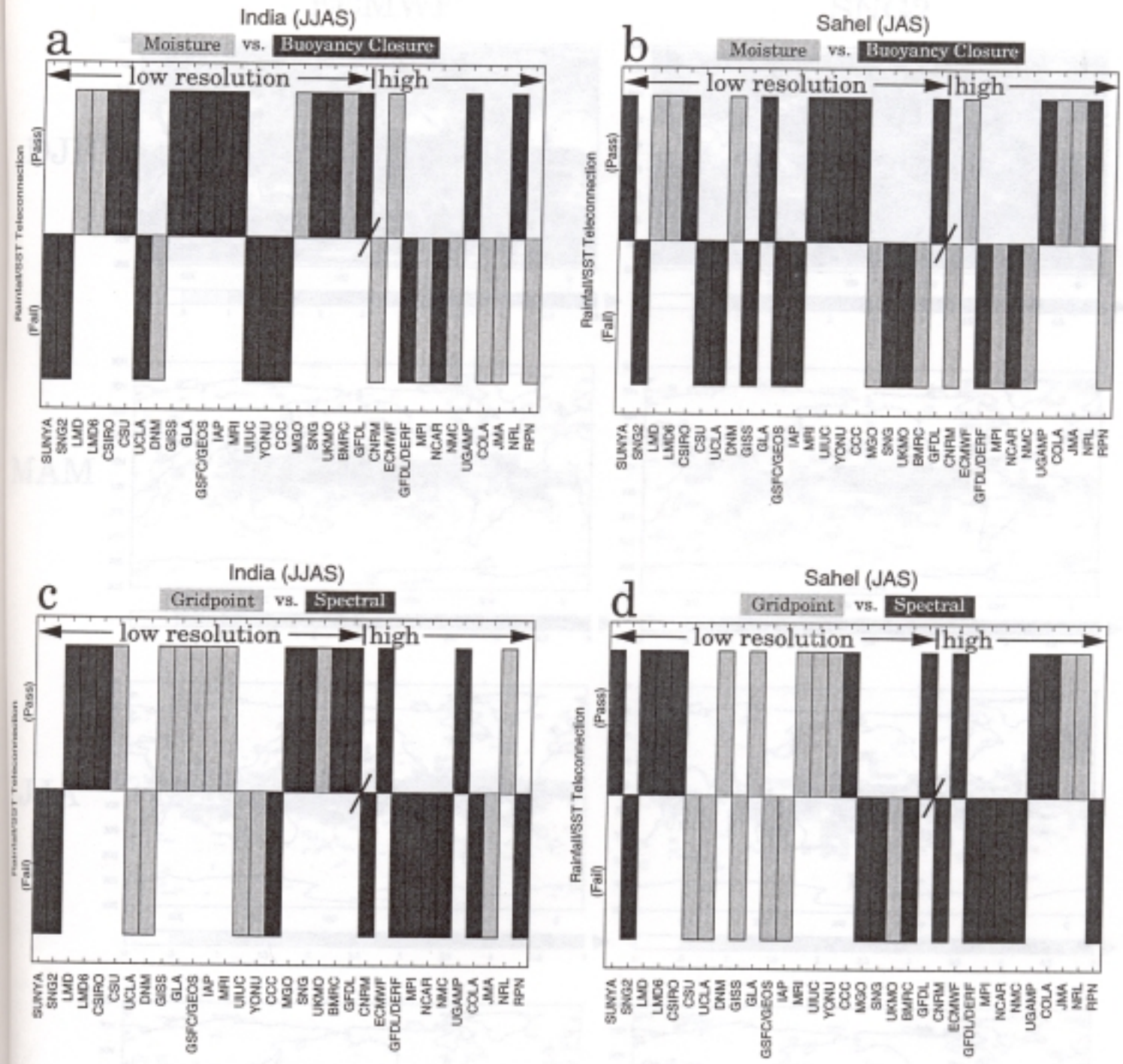
a
India (JJAS)
Moisture vs. Buoyancy Closure
low resolution
high
Rainfall/SST Teleconnection
(Pass)
(Fail)
SUNYA
SNG2
LMD
LMD6
CSIRO
CSU
UCLA
DNM
GISS
GLA
GSFC/GEOS
IAP
MRI
UIUC
YONU
CCC
MGO
SNG
UKMO
BMRC
GFDL
CNRM
ECMWF
GFDL/DERF
MPI
NCAR
NMC
UGAMP
COLA
JMA
NRL
RPN
b
Sahel (JAS)
Moisture vs. Buoyancy Closure
low resolution
high
Rainfall/SST Teleconnection
(Pass)
(Fail)
c
India (JJAS)
Gridpoint vs. Spectral
low resolution
high
d
Sahel (JAS)
Gridpoint vs. Spectral
low resolution
high

Fig. 21. Reproducibility of seasonally averaged precipitation (December/January/February, March/April/May, June/July/August, and September/October/November) for the ECMWF and SUNY/NCAR Genesis 2 initial condition sensitivity integrations. For values of R exceeding 0.45, the null hypothesis that SST has no influence may be rejected at the 5% level (Rowell 1995, personal communication).

ECMWF SNG2

)JF

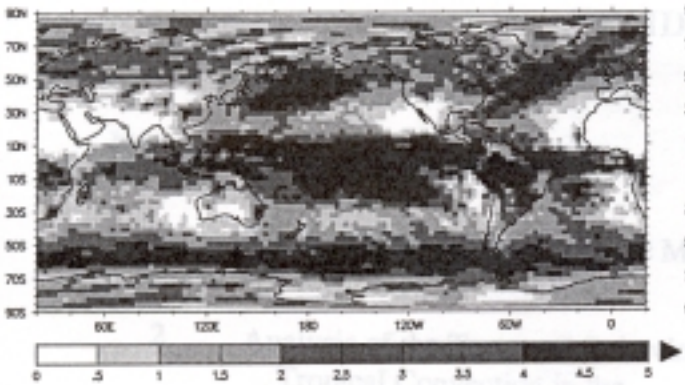

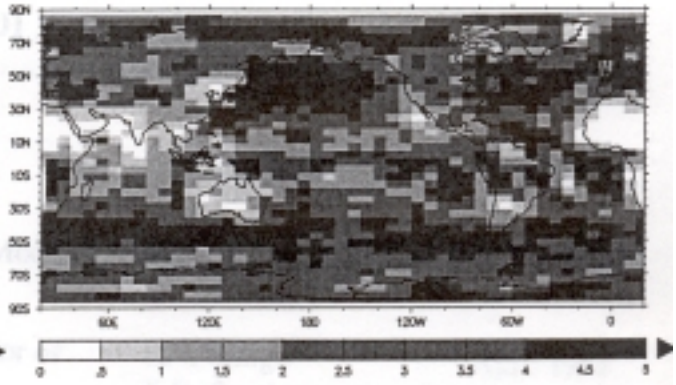

AM

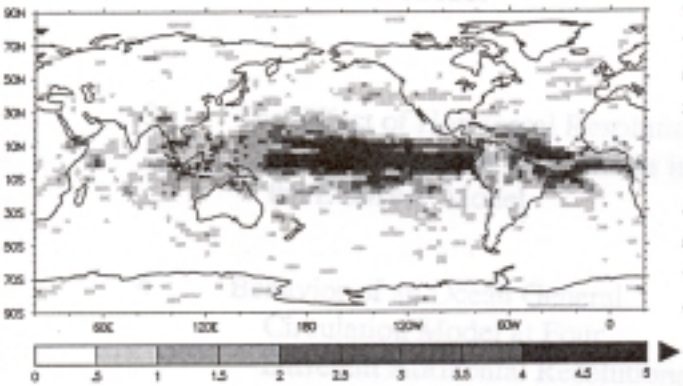

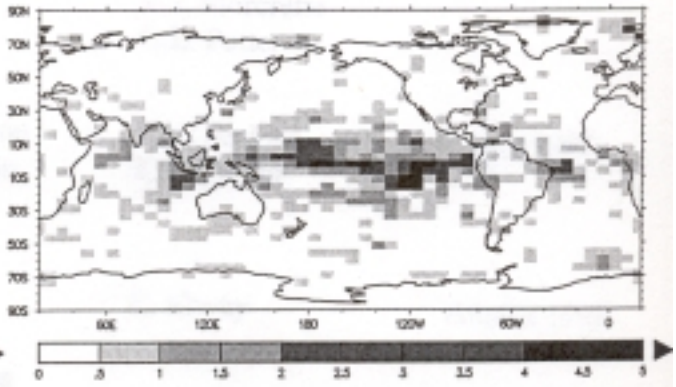

JA

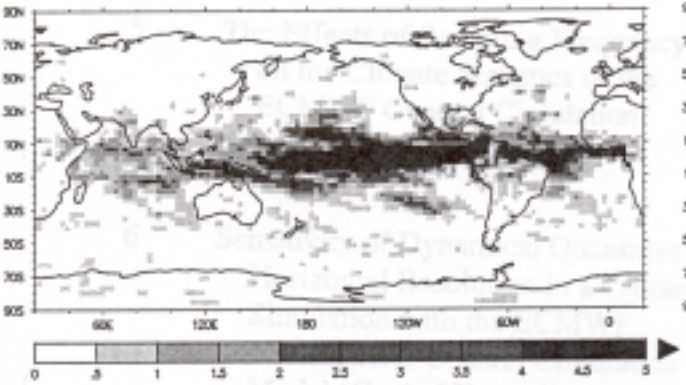

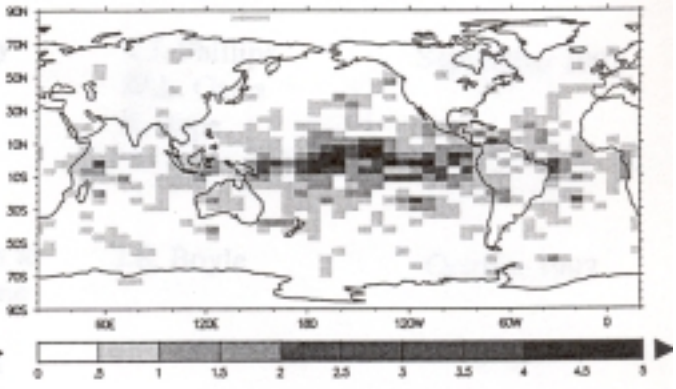

)N